Haptic Simulation, Perception and Manipulation of Deformable Objects

N. Magnenat-Thalmann[1], P. Volino[1], U. Bonanni[1], I.R. Summers[2], A. C. Brady[2], J. Qu[2], D. Allerkamp[3], M. Fontana[4], F. Tarri[4], F. Salsedo[4], M. Bergamasco[4]

[1] MIRALab, University of Geneva, Switzerland
[2] Biomedical Physics Research Group, University of Exeter, U.K.
[3] WelfenLab, Leibniz Universität Hannover, Germany
[4] PERCRO, Scuola Superiore Sant'Anna, Italy

Abstract

This tutorial addresses haptic simulation, perception and manipulation of complex deformable objects in virtual environments (VE). We first introduce HAPTEX, a research project dealing with haptic simulation and perception of textiles in VEs. Then, we present state-of-the-art techniques concerning haptic simulation and rendering, ranging from physically based modelling to control issues of tactile arrays and force-feedback devices. In the section on cloth simulation for haptic systems we describe techniques for simulating textiles adapted to the specific context of haptic applications. The section concerning tactile aspects of virtual objects shows how arrays of contactors on the skin can be used to provide appropriate spatiotemporal patterns of mechanical excitation to the underlying mechanoreceptors. Finally, the last section addresses the problem of developing suitable force feedback technologies for the realistic haptic rendering of the physical interaction with deformable objects, addressing the design of novel force feedback systems, innovative concepts for curvature simulation and control algorithms for accuracy improvement.

Categories and Subject Descriptors (according to ACM CCS): I.3.7 [Computer Graphics]: Virtual Reality

1. Introduction

Research on multimodal simulation in virtual environments faces the challenge of reproducing the aspect and behaviour of real objects. The simulation should be as realistic as possible and take place within a virtual reality (VR) system which provides the user with multiple interfacing modes (such as vision, audio, and interaction devices). Multimodality typically addresses the stimulation of different channels of perception. In this context, some perceptual channels have been more exploited than others. The achievement of a high degree of **visual** realism is increasingly becoming more popular in the entertainment industry, where video games are offering an always improved experience to the user. This is particularly supported by the establishment of dedicated Graphics Processing Units (GPUs) included in high-end graphics cards featuring programmable shaders. Also 3D spatialised **sound** has become common in the last years, and audio surround facilities in CAVE systems and even in home theatres are widely used. The ability to **touch** virtual objects, however, has not been fully exploited so far. The integration of realistic force-feedback and tactile stimulation within virtual reality applications is far less satisfying than audio-visual integration, and still at the beginning.

This tutorial deals with the reproduction of the sense of touch within virtual reality environments. In this context, we will present how to simulate, perceive and manipulate complex deformable objects such as virtual textiles both from the visual and the haptic viewpoint.

1.1 Reproducing the sense of touch

The discipline dealing with technology interfacing the user via the sense of touch is called **haptics**. A main obstacle to the widespread adoption of haptic devices within ordinary VR systems is currently represented by the unavailability of efficient-and-affordable haptic devices. But there are also other factors which preclude the application development in this domain, such as the high complexity and computational costs linked to haptic simulation.

In order to be performed accurately, multimodal simulation addressing vision and touch involves a high load on the computer's processing units. It is therefore important to find the best trade-off between the simulation's realism (in terms of visual and physical accuracy) and performance (in terms of response latency). To optimize the resource management, the visual and the haptic sensory channels can be processed in separate layers, since they have different requirements in terms of update rates or relevant physical properties to be simulated. However, this practice requires a robust and stable coupling between the two modalities [AH98]. The synchronization between layers must occur in real time, because delays or asynchronous behaviour can strongly affect the believability of the user experience.

1.2 Rendering complex deformable objects

The research concerning new ways of rendering virtual objects both visually and haptically in a fast and stable way represents a particular challenge when dealing with

physically based, complex deformable objects. In this field, researchers need to reproduce the object's aspect and behaviour in a physically accurate way and provide a simulation model able to calculate the deformations of the object occurring during interaction. Typically, the simulated interaction is tool-based, i.e. the user interacts with the object indirectly, feeling the forces arising during manipulation only at one specific point.

Complexity increases in the case of multipoint interactions, as collisions and deformations must be computed for each contact point. Direct haptic interaction, e.g. the simulation of the real contact between the human hand and a deformable object, is very demanding not only because of the number of deformations arising all over the contact surface and affecting each other, but also because of the technical difficulties in rendering the contact forces over a distributed area.

The haptic response rendered to the user of a multimodal simulation system can be of different nature. In this tutorial, we deal mainly with tactile and kinaesthetic feedback. Tactile arrays can reproduce the properties and small scale details of the object properties by selectively stimulating the mechanoreceptors under the skin of the fingertips. Tactile arrays give a feedback to the user, but do not allow him to exert actively forces. Force-feedback devices, in contrast, allow the user to add energy to the multimodal simulation system and actively manipulate virtual objects. Moreover, force-feedback devices reflect forces acting on the simulated object and allow the user to obtain kinaesthetic feedback about the performed operations.

2. Touching virtual textiles

Textile is an ideal deformable object to render in the context of haptic simulation. Humans are inherently familiar with clothes, and used to handle clothing materials since prehistoric ages. However, while cloth simulation is a popular topic in computer graphics, there have been very little attempts to render textiles haptically [GPU*03] [Hua02]. In these cases, only static cloth has been taken into consideration. Animated textiles were not taken into account because of the high requirements posed by the real time animation of cloth.

Interestingly, these early attempts have tried to combine the results of studies on physical properties of fabrics done in the textile industry with garment simulation. However, only a very limited amount of fabric parameters was taken into consideration. This can be easily ascribed to one of the limitations we face today in the field of computer graphics and haptics: the high number of physical properties we are able to feel and discriminate with our sensorial system can't be realistically and exhaustively reproduced by a multimodal simulation system today. These limitations concern both the visual and the haptic aspect of the simulation, and affect not only textiles but all kinds of physically based deformable objects. It is therefore necessary to simplify the usage of physical parameters by identifying a finite number of properties that can be considered the most relevant for an approximate but realistic simulation of the handling of a specific deformable object. Moreover, this simplification is necessary for each channel of perception, since the description of an object's behaviour from the visual, tactile or kinaesthetic aspect has different requirements.

2.1 The HAPTEX Project

The European research project HAPTEX (HAPtic sensing of virtual TEXtiles) tackles several of the above mentioned challenges. The goal of HAPTEX is to provide a multimodal system able to simulate virtual textiles in real time, allowing multipoint haptic interaction with a piece of virtual fabric [SFR*05]. In the HAPTEX system, haptic manipulation takes place through a novel haptic interface, which provides both force- and tactile feedback and aims to reproduce the feeling of touching a cloth surface with two fingertips.

Figure 1: *The HAPTEX showcase*

The system simulates the large-scale motion of a square of fabric hanging from a stand in virtual space, accurately described by its mechanical properties (such as stiffness or elasticity). These large-scale forces are returned by a force feedback device which allows for haptic manipulation. Moreover, tactile stimuli are derived from the fabric's small scale properties (texture and roughness) and rendered by piezoelectric tactile arrays integrated in the force-feedback device.

Users of the HAPTEX System can perform actions such as touching, stroking and stretching the virtual garment, selecting the simulated textile from a range of samples and feeling the different physical characteristics between them. The HAPTEX System allows to perform different textile handling actions, depicted in the following figure.

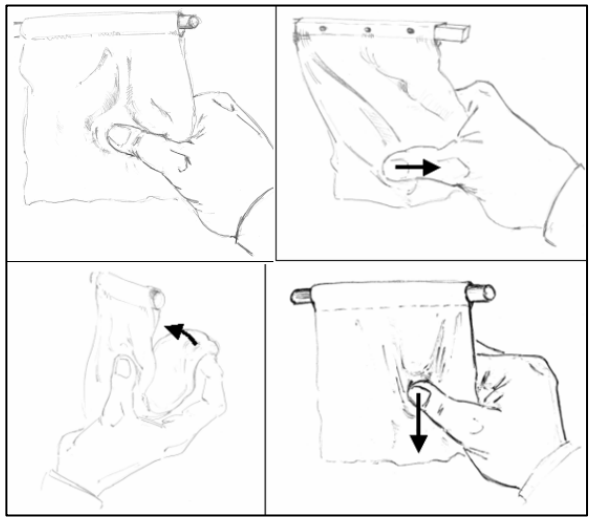

Figure 2: *Envisaged handling actions*

2.2 Design of the haptic system

In the HAPTEX System, both the visual simulation and the haptic rendering are based on the physical properties of real textiles. Modelling the behaviour of textiles is a complex task because of its dependency on several parameters such as flexibility, compressibility, elasticity, resilience, density, surface contour (roughness, smoothness), surface friction and thermal character [MMLMT05]. The process of handling fabrics to understand their properties and structure is called "fabric hand". Understanding the way people are used to handle the objects to simulate (in this case, textiles) is of crucial relevance for designing and developing a haptic system. The HAPTEX approach is to analyze all perceptual and practical implications of fabric hand, in order to derive a set of requirements to the system. From these ideal requirements, the system is realized according to the possibilities offered by today's technology [Hap06a]. The research and developments done in the context of the HAPTEX project cover textile measurements, real-time cloth simulation, tactile interfaces, force-feedback devices, haptic rendering (both tactile and force-feedback) and the integration of the complete haptic system.

2.3 Components of the HAPTEX System

The HAPTEX System is mainly composed by the following components [MTB06] [Hap05a]:

Measured physical parameters: The "Kawabata Evaluation System for Fabrics" (KES-F) is one of the main standards in the field of objective measurements of fabric hand [Kaw80]. The KES-F equipment is able to test for textile properties and extract physical parameters of textiles. These vary depending on the fibre type or fabric type and dimension [Hap05b]. Alternatively, other equipments such as tensile testers can be used to obtain specific physical parameters of fabric samples [MMLMT05]. The physical parameters are used by the cloth simulation, the tactile renderer and the force-feedback renderer.

Cloth simulation: The HAPTEX textile simulation is driven by a mechanical model which takes as input part of the mechanical parameters obtained from measurements on fabrics [VDB*07]. See Section 3 for more details.

Tactile component: The tactile array generates impulses of mechanical excitation for the mechanoreceptors underlying the skin of the user's fingertip. These spatiotemporal stimuli evoke the sensation of stroking the finger over a surface and feeling its patterns and edges. A tactile renderer returns drive signals for the array on the basis of the user's movements and a model of the finger/object interaction [Hap06a] [Hap06b]. See Section 4 for more details.

Force-feedback component: The force-feedback device returns to the user the forces acting on the manipulated piece of textile. A force-feedback renderer takes care of the computation of forces to be returned on the basis of the mechanical model of the cloth simulation. The force-feedback device also hosts the tactile component. Different configurations of the force-feedback component have been realized in the context of the HAPTEX Project [Hap06a] [Hap06b]. See Section 5 for more details.

3. Cloth Simulation in Haptic Systems

As any simulation system, cloth simulation requires significant computational resources for being performed accurately. Its integration in real-time simulation systems requires the implementation of state-of-the-art techniques, for mechanical models as well as for numerical integration. Furthermore, haptic applications require high robustness for dealing with approximate tracking and highly variable frame rates inherent to the performance and artefacts of current motion tracking devices. In this section, we describe some techniques for cloth simulation adapted to the specific context of haptic applications.

3.1 Overview

Garment simulation for interactive applications still remains a challenge, and the challenge is mainly to combine state-of-the-art simulation techniques that offer the best trade-off between computational speed, accuracy and robustness.

The particular challenges are described in the following sections. These are mainly:

* The design of a fast simulation system for simulating the tensile and bending elastic properties of cloth materials, which may possibly be anisotropic and nonlinear.

* The implementation of an efficient numerical integrator that offers robust simulation ensuring stability despite possible irregular frame rates and other artefacts related to motion tracking techniques.

3.2 Simulating the Mechanics of Cloth

3.2.1 Mechanical Properties of Cloth

The mechanical properties of deformable surfaces can be grouped into four main families:

* **Elasticity**, which characterizes the internal forces resulting from a given geometrical deformation.

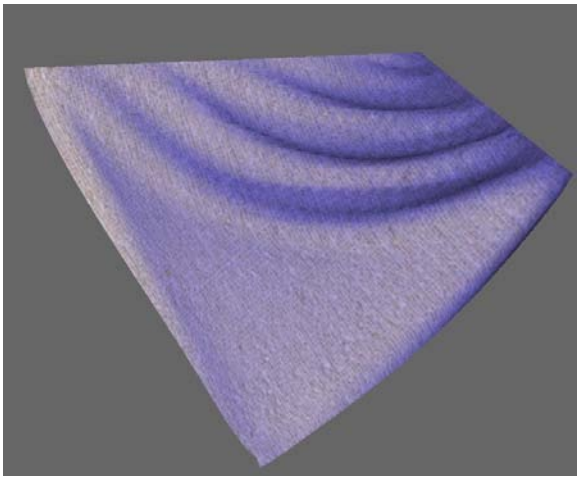

Figure 3: *Piece of textile simulated in real-time*

* **Viscosity**, which includes the internal forces resulting from a given deformation speed.

* **Plasticity**, which describes how the properties evolve according to the deformation history.

Most important are the elastic properties that are the main contributor of mechanical effects in the usual contexts where cloth objects are used. In the context of haptic applications, the motion of the cloth also depends on

dissipative effects related to viscosity and plasticity, which therefore have to be taken into account up to some degree of approximation by the simulation system.

Depending on the amplitude of the mechanical phenomena under study, the curves expressing mechanical properties exhibit shapes of varying complexity. If the amplitude is small enough, these shapes may be approximated by straight lines. This **linearity** hypothesis is a common way to simplify the characterization and modelling of mechanical phenomena.

It is common in elasticity theory to consider that the orientation of the material has no effect on its mechanical properties (**isotropy**). This however is inappropriate for cloth, as its properties depend considerably on their orientation relative to the fabric thread.

Elastic effects can be divided into several contributions:

* **Metric elasticity**, deformations along the surface plane.

* **Bending elasticity**, deformations orthogonally to the surface plane.

Metric elasticity is the most important and best studied aspect of fabric elasticity. It is usually described in terms of strain-stress relations. For linear elasticity, the main laws relating the strain e to the stress s involve three parameters, which are:

* **The Young modulus E**, summarizing the material's reaction along the deformation direction.

* **The Poisson coefficient ν**, characterizing the material's reaction orthogonal to the deformation direction.

* **The Rigidity modulus G**, pertaining to oblique reactions.

Along the two orthogonal directions **i** and **j**, these relations, named **Hook's Law**, **Poisson Law** and **Simple Shear Law** relating the stress **ε** to the strain **σ** are respectively expressed as follows:

$$\varepsilon_{ii} = \frac{1}{E_i}\sigma_{ii} \qquad \varepsilon_{jj} = \frac{\nu_{ij}}{E_i}\sigma_{ii} \qquad \varepsilon_{ij} = \frac{1}{G_{ij}}\sigma_{ij} \tag{1}$$

Cloth materials are two-dimensional surfaces for which two-dimensional variants of the elasticity laws are suitable. They are not isotropic, but the two orthogonal directions defined by the thread orientations can be considered as the main orientations for any deformation properties. In these **orthorhombic** cloth surfaces, the two directions are called **weft** (**u**) and **warp** (**v**), and they have specific Young modulus and Poisson coefficients, $\mathbf{E_u}$, $\boldsymbol{\nu_u}$ and $\mathbf{E_v}$, $\boldsymbol{\nu_v}$ respectively. The elasticity law can be rewritten in terms of these directions as follows:

$$\begin{bmatrix}\sigma_{uu}\\ \sigma_{vv}\\ \sigma_{uv}\end{bmatrix} = \frac{1}{1-\nu_u\nu_v}\begin{bmatrix}E_u & \nu_v E_u & 0\\ \nu_u E_v & E_v & 0\\ 0 & 0 & G(1-\nu_u\nu_v)\end{bmatrix}\begin{bmatrix}\varepsilon_{uu}\\ \varepsilon_{vv}\\ \varepsilon_{uv}\end{bmatrix} \tag{2}$$

Energetic considerations imply the above matrix to be symmetric, and therefore the products $\mathbf{E_u}\,\boldsymbol{\nu_v}$ and $\mathbf{E_v}\,\boldsymbol{\nu_u}$ are equal. Considering isotropic materials, we also have the following relations:

$$E_u = E_v\nu_u = \nu_v G = \frac{E}{2(1-\nu)} \tag{3}$$

A similar formulation can be obtained for bending elasticity. However the equivalent of the Poisson coefficient for bending is usually taken as null. The relation between the curvature strain **τ** and stress **γ** is expressed using the flexion modulus **B** and the flexion rigidity **K** (often taken as null) as follows:

$$\begin{bmatrix}\tau_{uu}\\ \tau_{vv}\\ \tau_{uv}\end{bmatrix} = \begin{bmatrix}B_u & 0 & 0\\ 0 & B_v & 0\\ 0 & 0 & K\end{bmatrix}\begin{bmatrix}\gamma_{uu}\\ \gamma_{vv}\\ \gamma_{uv}\end{bmatrix} \tag{4}$$

While elasticity expresses the relation between the force and the deformation, viscosity expresses the relation between the force and the deformation speed in a very similar manner. To any of the elasticity parameters can be defined a corresponding viscosity parameter obtained by substitution of the stresses **ε** and **γ** by their derivatives along time **ε'** and **γ'**.

While the described linear laws are valid for small deformations of the cloth, large deformations usually enter the nonlinear behaviour of cloth, where there is no more proportionality between strain and stress. This is practically observed by observing a "limit" in the cloth deformation as the forces increases, often preceding rupture (resilience), or remnant deformations observed as the constraints are released (plasticity). A common way to deal with such nonlinear models is to assume weft and warp deformation modes as still being independent, and replace each linear parameter $\mathbf{E_u}$, $\mathbf{E_v}$, **G**, $\mathbf{B_u}$, $\mathbf{B_v}$ by nonlinear strain-stress behaviour curves.

3.2.2 Measuring the Mechanical Properties of Cloth

The garment industry needs the measurement of major fabric mechanical properties through normalized procedures that guarantee consistent information exchange between garment industry and cloth manufacturers. The **Kawabata Evaluation System for Fabric** (KES) is a reference methodology for the experimental observation of the elastic properties of the fabric material. Using five experiments, fifteen curves are obtained, which then allow the determination of twenty-one parameters for the fabric, among them all the linear elastic parameters described above, except for the Poisson coefficient.

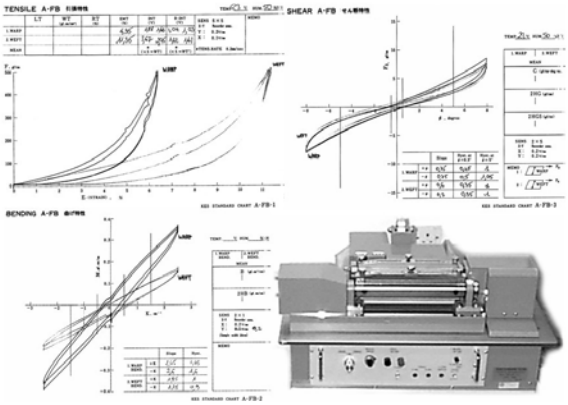

Figure 4: *Measuring cloth properties using KES.*

Five standard tests are part of KES for determining the mechanical properties of cloth, using normalized measurement equipment. The **tensile test** measures the force/deformation curve of extension for a piece of fabric of normalized size along weft and warp directions and allows the measurement of $\mathbf{E_u}$ and $\mathbf{E_v}$ along with other parameters assessing nonlinearity and hysteresis. The **shearing test** is the same experiment using shear deformations, which allows the measurement of **G**. The **bending test** measures the curves for bending deformation in a similar way, and allows the measurement of $\mathbf{B_u}$ and $\mathbf{B_v}$. Finally, the **compression test** and the **friction test** allow the measurement of parameters related to the compressibility and the friction coefficients.

While the KES measurements allow determination of parameters assessing the nonlinearity of the behaviour curves and some evaluation of the plasticity, other methodologies, such as the FAST method, use simpler procedures to determine the linear parameters only.

While the Kawabata measurements and similar systems summarize the basic mechanical behaviours of fabric material, the visual deformations of cloth, such as buckling and wrinkling, are a complex combination of these parameters with other subtle behaviours that cannot be characterized and measured directly.

In order to take these effects into account, other tests focus on more complex deformations. Among them, the draping test considers a cloth disk of given diameter draped onto a smaller horizontal disc surface. The edge of the cloth will fall around the support, and produce wrinkling. The wrinkle pattern can be measured (number and depth of the wrinkles) and used as a validation test for simulation models.

Tests have also been devised for measuring other complex deformation of fabric material, mostly related to bending, creasing and wrinkling.

3.3 Cloth Simulation Systems

Cloth being approximated as a thin surface, its mechanical behaviour is decomposed in in-plane deformations (the 2D deformations along the cloth surface plane) and bending deformation (the 3D surface curvature).

The in-plane behaviour of cloth is described by relationships relating, for any cloth element, the stress $\boldsymbol{\sigma}$ to the strain $\boldsymbol{\varepsilon}$ (for elasticity) and its speed $\boldsymbol{\varepsilon}'$ (for viscosity) according the laws of viscoelasticity. For cloth materials, strain and stress are described relatively to the weave directions weft and warp following three components: weft and warp elongation (**uu** and **vv**), and shear (**uv**). Thus, the general viscoelastic behaviour of a cloth element is described by strain-stress relationships as follows:

$$\begin{aligned}
&\sigma_{uu}(\varepsilon_{uu},\varepsilon_{vv},\varepsilon_{uv},\varepsilon_{uu}',\varepsilon_{vv}',\varepsilon_{uv}')\\
&\sigma_{vv}(\varepsilon_{uu},\varepsilon_{vv},\varepsilon_{uv},\varepsilon_{uu}',\varepsilon_{vv}',\varepsilon_{uv}')\\
&\sigma_{uv}(\varepsilon_{uu},\varepsilon_{vv},\varepsilon_{uv},\varepsilon_{uu}',\varepsilon_{vv}',\varepsilon_{uv}')
\end{aligned} \qquad (5)$$

Assuming to deal with an orthotropic material (usually resulting from the symmetry of the cloth weave structure relatively to the weave directions), there is no dependency between the elongation components (**uu** and **vv**) and the shear component (**uv**). Assuming null Poisson coefficient as well (a rough approximation), all components are independent, and the fabric elasticity is simply described by three independent elastic strain-stress curves (weft, warp, shear), along with their possible viscosity counterparts.

In the same manner, viscoelastic strain-stress relationships relate the bending momentum to the surface curvature for weft, warp and shear. With the typical approximations used with cloth materials, the elastic laws are only two independent curves along weft and warp directions (shear is neglected), with their possible viscosity counterparts.

The issue is now to define a model for representing these mechanical properties on geometrical surfaces representing the cloth. These curved surfaces are typically represented by polygonal meshes, being either triangular or quadrangular, and regular or irregular.

Continuum mechanics are one of the schemes used for accurate representation of the cloth mechanics. Mechanical equations are expressed along the curved surface, and then discretised for their numerical resolution. Such accurate schemes are however slow and not sufficiently versatile for handling large deformations and complex geometrical constraints (collisions) properly. Finite Element methods express the mechanical equations according to the deformation state the surface within well-defined elements (usually triangular or quadrangular). Their resolution also involves large computational charges. Another option is to construct a model based on the interaction of neighbouring discrete points of the surface. Such particle systems allow the implementation of simple and versatile models adapted for efficient computation of highly deformable objects such as cloth.

3.3.1 Spring-Mass Models

The simplest particle system one can think of is spring-mass systems. In this scheme, the only interactions are forces exerted between neighbouring particle couples, similarly as if they were attached by springs (described by a force/elongation law along its direction, which is actually a rigidity coefficient and a rest length in the case of linear springs). Spring-mass schemes are very popular methods, as they allow simple implementation and fast simulation of cloth objects. There has also been recent interest in this method as it allows quite a simple computation of the Jacobian of the spring forces, which is needed for implementing semi-implicit integration methods (see Section 3.4).

The simplest approach is to construct the springs along the edges of a triangular mesh describing the surface. This however leads to a very inaccurate model that cannot model accurately the anisotropic strain-stress behaviour of the cloth material, and also not the bending. More accurate models are constructed on regular square particle grids describing the surface. While elongation stiffness is modelled by springs along the edges of the grid, shear stiffness is modelled by diagonal springs and bending stiffness is modelled by leapfrog spring along the edges. This model is still fairly inaccurate because of the unavoidable cross-dependencies between the various deformation modes relatively to the corresponding springs. It is also inappropriate for nonlinear elastic models and large deformations. More accurate variations of the model consider angular springs rather than straight springs for representing shear and bending stiffness, but the simplicity of the original spring-mass scheme is then lost.

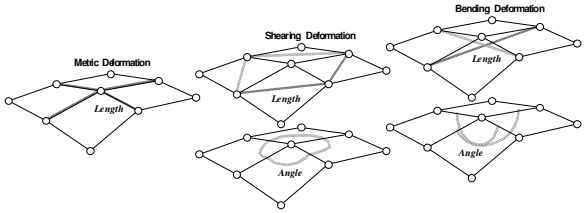

Figure 5: *Using length or angle springs for simulating cloth with a square particle system grid.*

3.3.2 Accurate Particle System for Tensile Viscoelasticity

Because of the real need of representing accurately the anisotropic nonlinear mechanical behaviour of cloth in garment prototyping applications, spring-mass models are inadequate, and we need to find out a scheme that really simulates the viscoelastic behaviour of actual surfaces. For this, we have defined a particle system model that relates this accurately over any arbitrary cloth triangle through simultaneous interaction between the three particles which are the triangle vertices. Such a model integrates directly and accurately the strain-stress model defined in Part 2.1 using polynomial spline approximations of the strain-stress curves, and remains accurate for large deformations.

In this model, a triangle element of cloth is described by 3 2D coordinates (**ua**, **va**), (**ub**, **vb**), (**uc**, **vc**) describing the location of its vertices **A**, **B**, **C** on the weft-warp coordinate system defined by the directions **U** and **V** with an arbitrary origin. They are orthonormal on the undeformed cloth (Figure M4). Out of them, a precomputation process evaluates the following values:

$$Rua = d^{-1}(vb - vc) \qquad Rva = -d^{-1}(ub - uc)$$
$$Rub = -d^{-1}(va - vc) \qquad Rvb = d^{-1}(ua - uc)$$
$$Ruc = d^{-1}(va - vb) \qquad Rvc = -d^{-1}(ua - ub)$$
$$\text{with}$$
$$d = ua(vb - vc) + ub(vc - va) + uc(va - vb) \qquad (6)$$

During the computation process, the current deformation state of the cloth triangle is evaluated using the current 3D direction and length of the deformed weft and warp direction vectors **U** and **V**. They are computed from the current positions **Pa**, **Pb**, **Pc** of its supporting vertices as follows:

$$U = Rua\ Pa + Rub\ Pb + Ruc\ Pc$$
$$V = Rva\ Pa + Rvb\ Pb + Rvc\ Pc \qquad (7)$$

The current in-plane strains **ε** of the cloth triangle is then computed with the following formula:

$$\varepsilon_{uu} = |U| - 1 \qquad \varepsilon_{vv} = |V| - 1$$
$$\varepsilon_{uv} = \frac{|U+V|}{\sqrt{2}} - \frac{|U-V|}{\sqrt{2}} \qquad (8)$$

We have chosen to replace the traditional shear deformation evaluation based on the angle measurement between the thread directions by an evaluation based on the length of the diagonal directions. The main advantage of this is a better accuracy for large deformations (the computation of the behaviour of an isotropic material under large deformations remains more axis-independent).

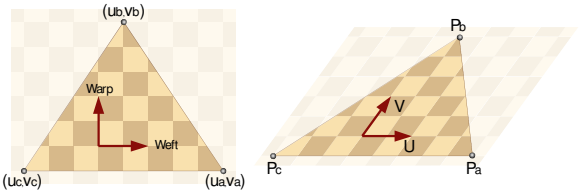

Figure 6: *A triangle of cloth element defined on the 2D cloth surface (left) is deformed in 3D space (right) and its deformation state is computed from the deformation of its weft-warp coordinate system.*

For applications that model internal in-plane viscosity of the material, the "evolution speeds" of the weave direction vectors are needed as well. They are computed from the current triangle vertex speeds **Pa'**, **Pb'**, **Pc'** as follows:

$$U' = Rua\ Pa' + Rub\ Pb' + Ruc\ Pc'$$
$$V' = Rva\ Pa' + Rvb\ Pb' + Rvc\ Pc' \qquad (9)$$

Then, the current in-plane strain speeds **ε'** of the triangle is computed:

$$\varepsilon_{uu}' = \frac{U \cdot U'}{|U|} \qquad \varepsilon_{vv}' = \frac{V \cdot V'}{|V|}$$
$$\varepsilon_{uv}' = \frac{(U+V)\cdot(U'+V')}{|U+V|\sqrt{2}} - \frac{(U-V)\cdot(U'-V')}{|U-V|\sqrt{2}} \qquad (10)$$

At this point, the in-plane mechanical behaviour of the material can be expressed for computing the stresses **σ** out of the strains **ε** (elasticity) and the strain speeds **ε'** (viscosity) using the curves discussed in Part 2.2. Finally, the force contributions of the cloth triangle to its support vertices computed from the stresses **σ** as follows:

$$Fa = -\frac{d}{2}\left((Rua\ \sigma_{uu} + Rva\ \sigma_{uv})\frac{U}{|U|} + (Rua\ \sigma_{uv} + Rva\ \sigma_{vv})\frac{V}{|V|} \right) \qquad (11)$$
$$Fb = -\frac{d}{2}\left((Rub\ \sigma_{uu} + Rvb\ \sigma_{uv})\frac{U}{|U|} + (Rub\ \sigma_{uv} + Rvb\ \sigma_{vv})\frac{V}{|V|} \right)$$
$$Fc = -\frac{d}{2}\left((Ruc\ \sigma_{uu} + Rvc\ \sigma_{uv})\frac{U}{|U|} + (Ruc\ \sigma_{uv} + Rvc\ \sigma_{vv})\frac{V}{|V|} \right)$$

It is important to note that when using semi-implicit integration schemes (see Section 3), the contribution of these forces in the Jacobian **∂F/∂P** and **∂F/∂P'** can easily be computed out of the curve derivatives **∂σ/∂ε** and the orientation of the vectors **U** and **V**.

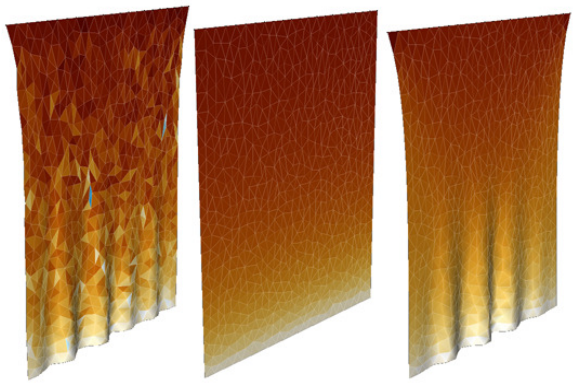

Figure 7: *Drape accuracy between a simple spring-mass system along the edges of the triangle mesh (left) and the proposed accurate particle system model (centre). Colour scale shows deformation. The spring-mass model exhibits inaccurate local deformations, along with an excessive "Poisson" behaviour. This is not the case with the accurate model, which may still model the "Poisson" effect if needed (right, with a Poisson coefficient 0.5). The spring-mass model is also unable to simulate anisotropic or nonlinear models accurately.*

3.3.3 Linear Particle System for Bending Elasticity

Unlike tensile stiffness, bending stiffness necessitates the action of out-of-plane forces that are usually more expensive to compute than in-plane forces.

Several solutions have been proposed in the literature, representing two main approaches. The first is to use crossover springs that extend the surface, opposing transversal bending. This approach, which integrates nicely in any simulation system based on spring-mass, is however very inaccurate. The second is to evaluate precisely the angle between adjacent mesh elements and to create between them normal forces that oppose this angle through opposite bending momentum. This approach can reach similar accuracy as grid continuum-mechanics and grid particle system derivatives which are fairly complex to evaluate. The third is to obtain a completely linear formulation of bending forces by computing it directly as a weighted sum of particle positions, without any consideration of the surface normals or any other complex geometric computation.

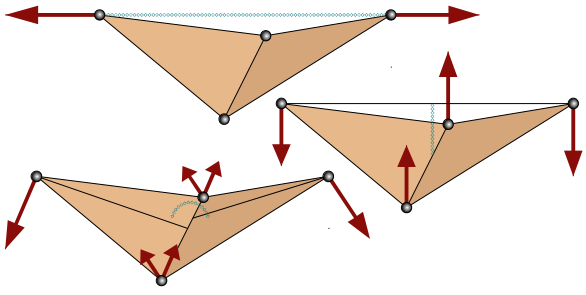

Figure 8: *Three ways for creating bending stiffness in a triangle mesh: Using tensile crossover springs over mesh edges (top), using forces along triangle normals (bottom), and, as we propose, using forces evaluated from a weighted sum of vertex positions (right).*

The idea of the linear model is the following: First, a "bending vector" that represents the bending of the surface is computed through a simple linear combination of particle positions. Then, it is redistributed as particle forces according to the bending stiffness of the surface. This scheme preserves total translational and rotational momentum conservation without the need of recomputing the distribution coefficients according to the current position of the particles. This leads to a very simple computation process which is perfectly linear, and thus very well adapted to implicit numerical integration.

We start from two adjacent triangles ($\mathbf{P_A}$,$\mathbf{P_C}$,$\mathbf{P_D}$) and ($\mathbf{P_B}$,$\mathbf{P_D}$,$\mathbf{P_C}$). Their common edge has a length noted $\mathbf{l}$ and their respective heights relatively to vertices $\mathbf{P_A}$ and $\mathbf{P_B}$ are noted $\mathbf{h_A}$ and $\mathbf{h_B}$.

The two adjacent triangles approximate a curved surface that contains the four vertices of the two triangles, and we assume that the surface is only curved *orthogonally* to the edge ($\mathbf{P_C}$,$\mathbf{P_D}$) (Figure M2 left). This is indeed not an obvious assumption, since *any kind* of surface curvature may produce some bending around the edge. However, this choice can be assumed as being the best, as the direction of the edge bending matches the curvature of the surface.

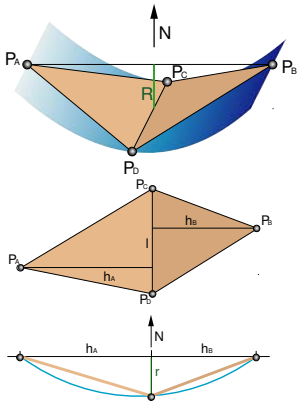

Figure 9: *The curved surface equivalent to two adjacent triangles (left), and the computation of its curvature (right).*

Our goal is now to estimate this curvature from the *height difference* noted $\mathbf{r}$ between the edges ($\mathbf{P_A}$,$\mathbf{P_B}$) and ($\mathbf{P_C}$,$\mathbf{P_D}$). As we restrict ourselves to linear bending, we assume that the bending stiffness remains constant whatever the amount of curvature, and therefore we evaluate it assuming the edge angle between the adjacent triangles remain small. In these conditions, we can evaluate the curvature $\boldsymbol{\gamma}$ of the surface as follows:

$$\gamma = \frac{2\,r}{h_A\,h_B} \qquad (12)$$

Now, we need to compute the height difference $\mathbf{r}$ from the current position of the triangles. Again in the context of small edge angle, this is approximated through the projected length of a *bending vector* $\mathbf{R}$ on the approximate normal of the surface $\mathbf{N}$ (normalized to unit length) so as:

$$r = R \cdot N \qquad (13)$$

The bending vector $\mathbf{R}$ indeed represents a kind of "second-order deformation difference" between the two elements, and its normal component represents the actual surface bending. It can be computed as a simple linear combination of vertex positions, as follows:

$$R = \alpha_A\ P_A + \alpha_B\ P_B + \alpha_C\ P_C + \alpha_D\ P_D \qquad (14)$$

With:

$$\alpha_A = \frac{|N_B|}{|N_A|+|N_B|} = \frac{h_B}{h_A+h_B} \qquad \alpha_C = -\frac{|N_D|}{|N_C|+|N_D|} \qquad (15)$$
$$\alpha_B = \frac{|N_A|}{|N_A|+|N_B|} = \frac{h_A}{h_A+h_B} \qquad \alpha_D = -\frac{|N_C|}{|N_C|+|N_D|}$$

Using the normals:

$$N_A = (P_A - P_C) \wedge (P_A - P_D) \qquad N_C = (P_C - P_B) \wedge (P_C - P_A) \quad (16)$$
$$N_B = (P_B - P_D) \wedge (P_B - P_C) \qquad N_D = (P_D - P_A) \wedge (P_D - P_B)$$

The main idea of our linear bending stiffness scheme is to apply forces on the particles that directly oppose the bending vector **R** of the current deformation, *without* projection along **N**, or any other intermediate computations that would explicitly evaluate the actual values of the bending strain and stress.

Thus, we consider that the bending forces $\mathbf{F_A}$, $\mathbf{F_B}$, $\mathbf{F_C}$, $\mathbf{F_D}$ are applied on the vertices $\mathbf{P_A}$, $\mathbf{P_B}$, $\mathbf{P_C}$, $\mathbf{P_D}$ respectively along the vector **R**. That can be done as follows, with a stiffness coefficient $\boldsymbol{\lambda}$ that would bring adequate scaling:

$$F_A = -\lambda\ \alpha_A\ R \qquad F_C = -\lambda\ \alpha_C\ R \qquad (17)$$
$$F_B = -\lambda\ \alpha_B\ R \qquad F_D = -\lambda\ \alpha_D\ R$$

This distribution, which uses the same coefficients as (14), has been chosen for satisfying total mechanical momentum conservation in the system.

Finally, we need to compute the value of the stiffness coefficient $\boldsymbol{\lambda}$ according to the linear bending stiffness modulus $\boldsymbol{\mu}$ of the surface and the geometry of the triangles.

The bending momentum created by the forces $\mathbf{F_A}$ and $\mathbf{F_B}$ applied on respectively $\mathbf{P_A}$ and $\mathbf{P_B}$ around the edge ($\mathbf{P_C}$,$\mathbf{P_D}$) can be expressed from the height difference **r**, through (17), (15) and (13) as follows:

$$h_A\ F_A \cdot N = -h_B\ F_B \cdot N = \lambda\ \frac{h_A\ h_B}{h_A+h_B}\ R \cdot N = \lambda\ \frac{h_A\ h_B}{h_A+h_B}\ r \qquad (18)$$

The bending momentum also results from the bending stiffness modulus $\boldsymbol{\mu}$ of the bent surface of curvature $\boldsymbol{\gamma}$ applied over the length **l** of the edge ($\mathbf{P_C}$,$\mathbf{P_D}$). From this, using (2):

$$l\ \mu\ \gamma = \frac{2\ l\ \mu\ r}{h_A\ h_B} \qquad (19)$$

A non-obvious issue is to take into account how adjacent edge bends combine together for describing the actual surface curvature. Energetic considerations, mainly detailed by [GHDS03] suggest that $\boldsymbol{\lambda}$ should be evaluated by equating (18) with *one third* of (19). Therefore:

$$\lambda = \frac{2}{3}\ \frac{h_A+h_B}{(h_A\ h_B)^2}\ l\ \mu \qquad (20)$$

It can be demonstrated that Only (14) and (17) are required for having exactly total mechanical momentum conservation, both translational and rotational, *whatever the current position of the particles* and whatever the actual way of computing coefficients, provided that their sum is null. Thus, momentum conservation is not broken by having the coefficients $\boldsymbol{\alpha_A}$, $\boldsymbol{\alpha_B}$, $\boldsymbol{\alpha_C}$, $\boldsymbol{\alpha_D}$ computed *independently* from the current position of the particles. Therefore, these should be precomputed using the initial shape of the mesh, or the parametric coordinates of the vertices on the cloth. In these conditions, the Jacobian of the bending stiffness forces is simple and straightforward to compute from (14) and (17) without any approximation. This is done as follows, with **I** denoting the identity matrix, and with any **J** and **K** among (**A**,**B**,**C**,**D**):

$$\frac{\partial F_J}{\partial P_K} = -\lambda\ \alpha_J\ \alpha_K\ I \qquad (21)$$

Thanks to a perfectly linear bending model, the Jacobian of all bending forces is constant and totally independent from the current particle positions. This allows efficient numerical resolution through usual implicit numerical resolution methods with good convergence properties, along with possible algorithmic optimizations for performing the computation quickly.

3.4 Numerical Integration

The equations resulting from the mechanical formulation of particle systems do usually express particle forces **F** depending on the state of the system (particle positions **P** and speeds **P'**). In turn, particle accelerations **P''** is related to particle forces **F** and masses **M** by Newton's 2nd law of dynamics. This leads to a second-order ordinary differential equation system, which is turned to first-order by concatenation of particle position **P** and speed **P'** into a state vector **Q**. A vast range of numerical methods has been studied for solving this kind of equations.

We have conducted extensive tests for benchmarking numerous integration methods, using performance, accuracy, stability and robustness as criteria. We have selected three candidates, each of which performs best in its own context:

* *1st-order semi-implicit Backward Euler*, which seems to be the best robust general-purpose method for any relaxation task (garment assembly and draping) [BHW94] [MDDB00].
* *2nd-order semi-implicit Backward Differential Formula*, which offers increased dynamic accuracy along time (garment simulation on animated characters), at the expense of robustness (unsuited for draping during interactive design) [EDC96].
* *5th-order explicit Runge-Kutta with timestep control*, which offers very high non-dissipative dynamic accuracy (accurate simulation of viscous and dissipative parameters in animated garments), at the expense of computation time (requires small time steps depending on the numerical stiffness, unsuited for stiff materials and refined discretisations) [BWH*06].

Our implementation integrates these three methods, and dynamically switches between them depending on the simulation context.

3.4.1 Discussing Integration Methods

3.4.1.1. Implicit Integration Methods

The most widely-used method for cloth simulation is currently the semi-implicit Backward Euler method, which was first used by Baraff et al in the context of cloth simulation. As any implicit method, it alleviates the need of high accuracy for the simulation of stiff differential equations, offering convergence for large timesteps rather

than numerical instability (a step of the semi-implicit Euler method with "infinite" timestep is actually equivalent to an iteration of the Newton resolution method) .

The formulation of a generalized implicit Euler integration is the following:

$$Q_{(t+dt)} - Q_{(t)} = Q'_{(t+\alpha\, dt)}\, dt \qquad (22)$$

The derivative value is not known at a moment after **t**, and is then extrapolated from the value at moment **t** using the Jacobian, leading to the semi-implicit expression which requires the resolution of a linear system:

$$Q_{(t+dt)} - Q_{(t)} = \left(I - \alpha \frac{\partial Q'}{\partial Q}_{(t)} dt \right)^{-1} Q'_{(t)}\, dt \qquad (23)$$

We have introduced the coefficient α so as to modulate the "implicitiсy" of the formula. Hence, $\alpha = 1$ is the regular implicit Backward Euler step (stable), whereas $\alpha = 0$ is the explicit Forward Euler step (unstable), and $\alpha = 1/2$ is the 2nd-order implicit Midpoint step (most accurate, at the threshold of stability).

The α parameter is a good handle for adjusting the compromise between stability and accuracy. While maximum robustness is obviously observed for large values, reducing its value increases accuracy (reduces numerical damping) at the expense of stability, and speeds up the computation as well (better conditioning of the linear system to be resolved).

Better accuracy can also be obtained through the use of the 2nd-order Backward Differential Formula (BDF-2), as described by Hauth et al. This uses the previous state of the system for enhancing accuracy up to 2nd-order, with a minimal impact on the computation charge. Its generalized implicit expression is:

$$Q_{(t+dt)} - Q_{(t)} = \beta \left(Q_{(t)} - Q_{(t-dt)} \right) + Q'_{(t+\alpha\, dt)}\, \delta t$$

$$\text{with} \quad \beta = \frac{2\alpha - 1}{2\alpha + 1} \quad \text{and} \quad \delta t = \frac{2}{2\alpha + 1} dt \qquad (24)$$

And its semi-implicit expression is:

$$Q_{(t+dt)} - Q_{(t)} = \left(I - \alpha \frac{\partial Q'}{\partial Q}_{(t)} \delta t \right)^{-1} \left(\beta \left(Q_{(t)} - Q_{(t-dt)} \right) + Q'_{(t)}\, \delta t \right) \qquad (25)$$

While $\alpha = 1$ is the regular implicit BDF-2 step, $\alpha = 0$ is the explicit Leapfrog method, and $\alpha = 1/2$ is again the implicit Midpoint method. Best accuracy is offered for $\alpha = 1/\sqrt{3}$, where the method is 3rd-order (moderately stable).

Compared to Backward Euler, the main interest of the BDF-2 method is that it exhibits better accuracy for dynamic simulation over time (less numerical damping) for moderately stiff numerical contexts (at the expense of reduced robustness for nonlinear situations). For very stiff contexts however, this benefit disappears. While it is possible to implement higher-order BDF methods, their interest is reduced by their lack of stability, and high accuracy could be more efficiently reached using high-order explicit methods. Stability of implicit methods is also affected by the nonlinearities of the mechanical model.

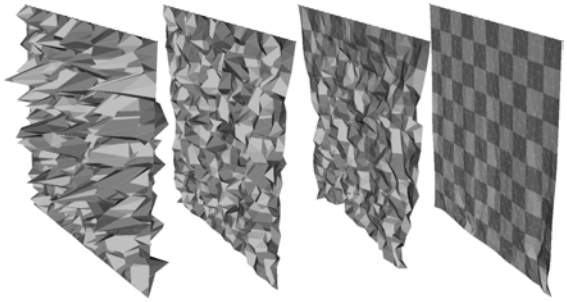

Figure 10: *Stability test: A square of cloth is initially deformed with large random perturbations, and then simulated using various timesteps.*

3.4.1.2. Explicit Integration Methods

Unlike implicit methods, explicit methods do not offer convergence to equilibrium if the timestep is too large compared to the numerical stiffness of the equations. On the other hand, they are very simple to implement, and much compute much faster than their implicit counterpart for reaching a given accuracy. This is particularly true for high-order methods, which offer very high accuracy if the timestep is small enough, but diverge abruptly if it exceeds a threshold (related to the stiffness of the equations). This is why an efficient timestep control scheme is essential for the implementation of these methods.

While the explicit 1st-order Euler and 2nd-order Midpoint methods should be restricted to simple applications (beside their simplicity, they have no benefits compared to their implicit counterparts), a popular choice is the 5th-order Runge-Kutta scheme with embedded error evaluation. It is a six-stage iteration process where the computed error magnitude can be used for controlling the adequate timestep very accurately, depending on accuracy and stability requirements. Unlike implicit methods, this method yields a very good guaranteed accuracy (resulting from the high-order, but which may require very small timesteps), which is particularly important for problems where energy conservation is a key issue (for example, evaluating the effect of viscous parameters in the motion of fabrics). On the other hand, explicit methods are quite unsuited for the fast relaxation of the static cloth draping applications.

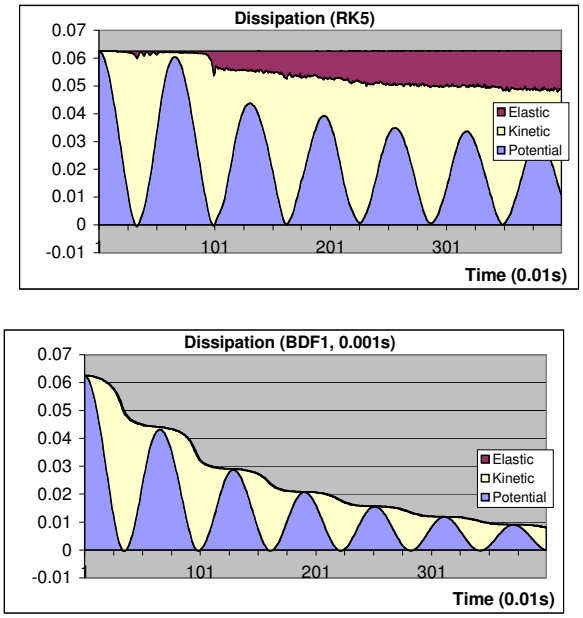

Figure 11: *Evaluation of numerical damping of various integration methods using energy dissipation plots along time(50cm x 50cm square cloth, initially horizontal, attached along one edge, linear isotropic 100N/m, 100g/m2, 2cm2 elements, no dissipative parameters). 5th-order Runge-Kutta (up) accurately preserves the total energy along time, a good amount of it being transferred to elastic energy through small-scale mesh jittering (timesteps between 0.0001s and 0.00001s). Implicit methods such as Inverse Euler (down) damp small-scale motion.*

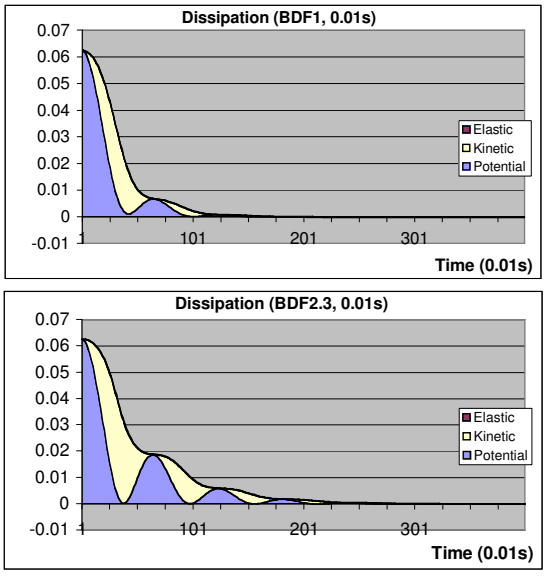

Figure 12: *The 3rd-order BDF2 variation (down) preserves energy significantly better than Inverse Euler (up).*

3.4.2 Implementation Issues

While there are no particular issues related to the implementation of explicit integration methods, semi-implicit methods require the resolution of large sparse linear equations systems, which are mainly constructed from the Jacobian of the mechanical law $\partial \mathbf{F}/\partial \mathbf{P}$ and $\partial \mathbf{F}/\partial \mathbf{P}'$ (their sparse structure relates the mechanical dependency between the particles). Among possible speed-up approximations, the Jacobian terms generated by the non-stiff forces can be neglected (they are then explicitly integrated).

A choice candidate for resolving this linear system is the Conjugate Gradient method, which is iterative and thus offers compromise between computation charge and symmetric accuracy, and which also allows efficient implementation for sparse systems.

Among possible optimizations are linearization schemes aimed at performing the computation using a constant approximation of the Jacobian, so as to implement pre-processing optimizations in the resolution. While giving reasonable benefits for draping applications, these approximations however generate large "numerical damping" that slow down convergence and alter highly the motion of the cloth along time.

The only solution for simulating the accurate motion of cloth was indeed to use real value of the Jacobian corresponding to the current state of the system. We have taken advantage of the Conjugate Gradient method which only needs the Jacobian matrix products with given vectors to compute these products "on the fly" directly from the system state, skipping the sparse explicit storage of the matrix for each frame. Our system actually allows performing partial linearization of the Jacobian, so as to use the linearization ratio offering the best trade-off between motion accuracy and stability, depending on the simulation context.

3.5 Collision Processing

Collision detection is indeed one of the most time-consuming tasks when it comes to simulate virtual characters wearing complete garments. In high-performance systems, this task is usually performed through an adapted bounding-volume hierarchy algorithm, which uses a constant Discrete-Orientation-Polytope hierarchy constructed on the mesh, and optimization for self-collision detection using curvature evaluation on the surface hierarchy. This algorithm is fast enough for allowing full collision and self-collision detection between all objects of the scene with acceptable impact on the processing time (rarely exceeds 20% of the total time). Thus, body and cloth meshes are handled totally symmetrically by the collision detection process, ensuring perfect versatility of the collision handling between the body and the several layers of garments.

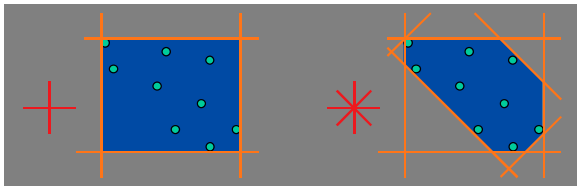

Figure 13: *Discrete-Orientation-Polytopes are a generalisation of axis-aligned Bounding Boxes.*

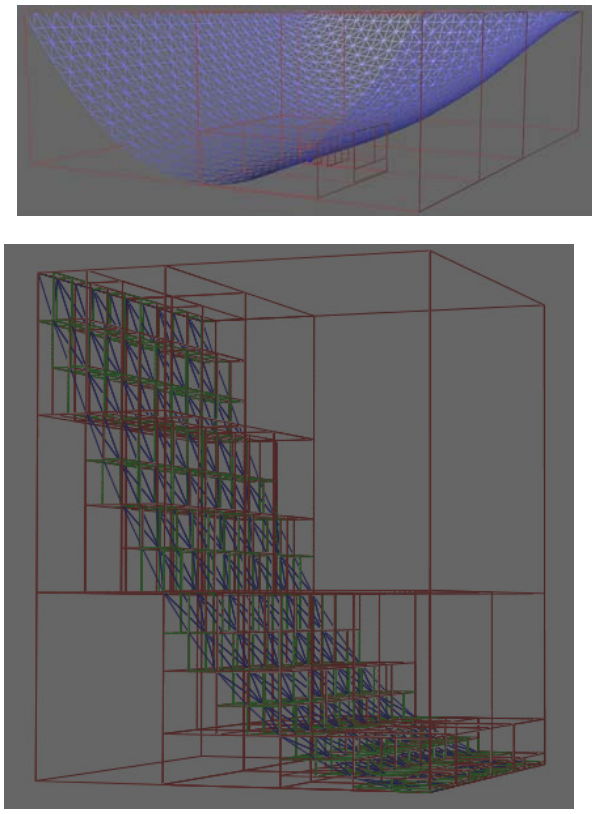

Figure 14: *Bounding-volume hierarchy for collision detection on a cloth mesh.*

Collision response is handled robustly using a geometrical scheme based on correction of mesh position, speed and acceleration. This scheme ensures good accuracy and stability without the need of large nonlinear forces that alter the numerical resolution of the mechanical model.

4. Tactile perception of Synthetic Surfaces

Tactile aspects of a virtual object can be represented as a spatial distribution of synthetic touch sensations over the fingertips. An array of contactors on the skin may be used to provide appropriate spatiotemporal patterns of mechanical excitation to the underlying mechanoreceptors. Tactile rendering software can generate drive signals for the array on the basis of the user's movements and a model of the finger/object interaction.

4.1 Overview

This section is concerned with the tactile aspects of a virtual object, represented as a spatial distribution of synthetic touch sensations over the fingertips. These sensations can provide information about the surface texture of the virtual object and about the contact between object and skin (contact area and position of edges/ corners).

To excite the skin mechanoreceptors, an array of contactors on the skin may be used to provide spatiotemporal patterns of mechanical input to the skin surface. In practice, such an array is one component of a haptic interface, integrated with a force-feedback component which represents the gross mechanical properties of the virtual object. Encounters with virtual objects, during active exploration of the workspace by the user, produce appropriate patterns of tactile stimulation on the fingertips. This is illustrated schematically in Figure 15.

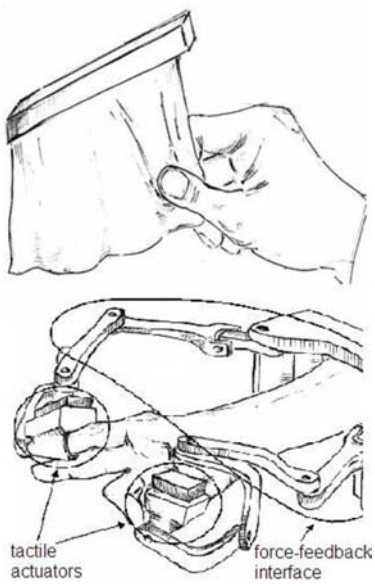

Figure 15: *Schematic diagram of a compound haptic interface. The upper picture shows a virtual scenario (from the HAPTEX project) in which a fabric sample is evaluated in terms of overall mechanical properties and surface properties; the lower picture indicates how the overall mechanical properties are represented by force-feedback and the surface properties are represented by tactile stimulation from actuators on the fingertips.*

When presenting the tactile aspects of a virtual object, the intention is not to reproduce the significant features of the small-scale surface topology of the object in terms of a virtual surface – that would require micron-scale resolution and is probably beyond the scope of current technology. Instead, the intention is to reproduce the perceptual consequences of small-scale features of the surface topology, i.e., appropriate excitation patterns over the various populations of touch receptors in the skin. (Shape displays have been developed to reproduce larger-scale features of an object's surface topology [WLH02, WLH04], at millimetre-scale resolution, but these are not the subject of the present discussion.)

4.2 Design of a stimulator array

As outlined above, an array of contactors on the skin may be used to provide spatiotemporal patterns of mechanical excitation to the underlying mechanoreceptors. The design requirements for such a stimulator array – contactor spacing, working bandwidth and output amplitude – are largely determined by the response of the mechanoreceptors.

The hairless skin which is found on the fingertips and the palms of the hands contains four populations of mechanoreceptors: pacinian receptors and three types of non-pacinian receptor [JYV00]. These populations differ in terms of their frequency response and their temporal response [GBH01]. Figure 16 indicates the distribution of pacinian receptors in the fingertip of a young adult.

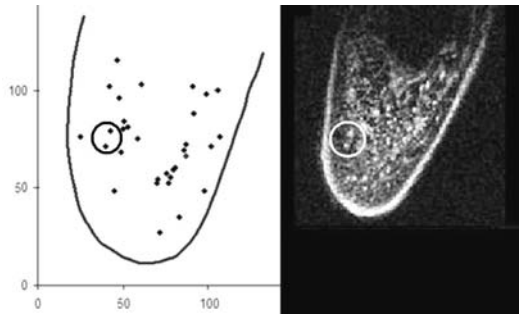

Figure 16: *Pacinian receptors in the fingertip. The left panel shows a 2D projection of receptor locations (140 μm units), identified from a set of MRI slices, one of which is shown in the right panel. For further details, see* [CSB*06].

The optimal spacing of contactors in a simulator array is determined by the spatial acuity of the sense of touch – around 1 mm on the fingertip [JYV00]. However, a contactor spacing of 1 mm equates to around 100 contactors over the fingertip, each of which requires independent control. This is realistic for a passive (non-moving) device [SC02, KBD*07] but is difficult to implement in an active device, for which a spacing of around 2 mm (i.e., around 25 contactors on the fingertip) may be a better choice. (There is some evidence [SCS*01] that perceptions available from an array with 2 mm spacing are not very different than those from an array with 1 mm spacing.)

In order to produce "realistic" touch sensations, a working bandwidth of around 10 to 500 Hz is required for the drive mechanism of each contactor, corresponding to the frequency range over which the various mechanoreceptors are sensitive [GBH01]. Pacinian receptors are expected to respond most strongly to frequencies in the upper part of this frequency range (100 to 500 Hz, say); stimulation at lower frequencies is expected to stimulate mainly non-pacinian receptors.

It is difficult to closely specify the amplitudes of contactor movement which are required to produce particular levels of touch sensation, because sensation level varies with the extent of the area stimulated, particularly when pacinian receptors are involved [Ver63]. However, it is possible to give approximate figures: "comfortable" sensation levels are produced by amplitudes of a few microns at frequencies around 300 Hz and a few tens of microns at frequencies around 50 Hz. (In one of very few studies on this topic, Verrillo *et al*. [VFS69] determined equal-sensation contours for a fixed area of stimulation on the palm of the hand,. It is not clear how well these data may be applied to the case of a variable area of stimulation on the fingertip.)

A further consideration is the direction of movement of the contactors in a stimulator array. In "real" touch perception, the interaction between skin and object produces normal and tangential forces on the skin surface (with two orthogonal components for the latter). However, stimulator arrays are constrained by present technologies to produce input forces in only a single direction (i.e., normal to the skin surface, or tangential in only one of the two available directions). It is difficult to assess the significance of this constraint. Since the aim is to produce appropriate excitation patterns over the various populations of touch receptors, the question is whether receptors that typically respond to forces in a particular direction in the "real" situation (e.g., receptors which respond to skin stretch caused by tangential forces) can be excited by forces in a different direction in the virtual situation. It is difficult to answer this question with certainty because the existing literature on mechanoreceptor transduction is very limited. In practice, it seems that the direction of contactor movement dose not make a great difference to the nature of the available tactile sensation, and so an acceptable stimulator can be designed on the basis of either tangential or normal movement.

Design requirements for contactor spacing, working bandwidth and output amplitude may be satisfied by a variety of electromechanical drive mechanisms. Hafez and colleagues [BHA*03, HB04] have developed arrays of drivers, based on shape-memory alloy or moving-coil technology, which apply normal forces to the skin. Hayward and colleagues [PH03, LPH07] have used piezoelectric-bimorph actuators to apply tangential forces. Summers *et al*. [SBS*05] have used similar actuators to apply normal forces, as have Kyung *et al*. [KAK*06].

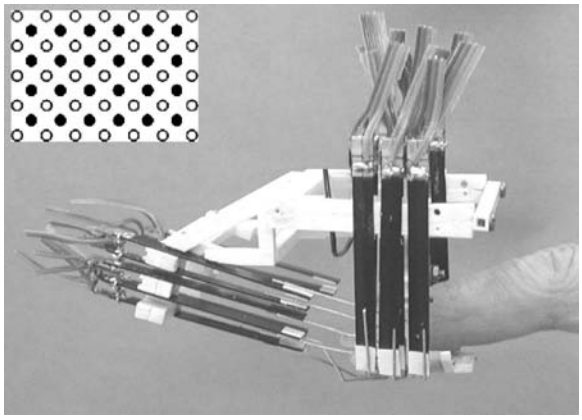

Figure 17: *Stimulator array developed for the HAPTEX project. The contactor surface lies under the finger – contactors are driven by piezoelectric bimorphs (appearing as black rectangles). The inset shows the arrangement of 24 moving contactors, interspersed between fixed contactors.*

Looking at one design of drive mechanism in more detail: the stimulator array developed for the HAPTEX project is shown in Figure 17. Piezoelectric bimorphs are used to drive 24 contactors in a 6 × 4 array on the fingertip, with a spacing of 2 mm between contactor centres. It can be seen that the drive mechanism is placed to the side of the finger and ahead of the finger, rather than below the contactor surface (which, at first sight, appears to be the mot convenient location). With one such array on the index finger and one on the thumb, this positioning of the drive mechanism allows the finger to move close to the thumb so that a virtual textile can be manipulated between the tips of finger and thumb.

The contactor surface delivers to the fingertip the small forces associated with touch stimuli, but it must also deliver the larger forces associated with the overall mechanical properties of the virtual object, represented by the output of the force-feedback system (see Figure 15). However, the moving contactors which provide touch stimuli are driven by delicate piezoelectric mechanisms and so they are unsuitable for delivering the force-feedback output, which may involve forces of considerable magnitude. Consequently, the contactor surface includes an additional set of contactors ("fixed" contactors – see inset to Figure 17) which deliver the force-feedback output, in parallel with the tactile stimulation from the moving contactors. This parallel delivery is shown schematically in Figure 18.

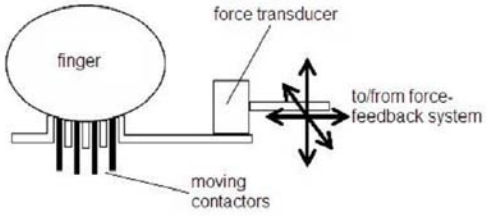

Figure 18: *Schematic diagram of the integration of the stimulator array and the force-feedback system. The finger rests on the contactor surface, composed of moving contactors (shown in black) which deliver tactile stimuli and "fixed" contactors (shown in white) which connect to the force-feedback system via a 3D force transducer.*

4.3 Drive signals for a stimulator array

During active exploration of a virtual tactile environment it is necessary to generate in real time a drive waveform for each contactor of the stimulator array(s) which are in contact with the user's fingertip(s). The amount of data which must be generated "on the fly" is thus considerable. For example, the HAPTEX system has 24-contactor arrays on finger and thumb, requiring 48 analogue drive signals, in principle each with a bandwidth of around 500 Hz. However, because of the limited temporal resolution, frequency resolution and phase sensitivity of human touch perception [She85, RHD*87, VGV90, FMF*92, SWM*05], there are possibilities for a significant reduction in the data flow. For example, each drive signal may be reduced to the sum of a limited number of sinusoidal components, distributed across the working bandwidth (10 to 500 Hz – see above). The drive signal may then be simply specified in terms of the amplitudes of these components, which require an update every 20 ms or so.

In the HAPTEX project, a cut-down version of this scheme has been used, in which the drive signal to each contactor is the sum of components at only two frequencies: 40 Hz and 320 Hz. Following the suggestion of Bernstein [BED89], the higher frequency was selected (at 320 Hz) to target pacinian receptors and the lower frequency was selected (at 40 Hz) to target non-pacinian receptors. Each drive signal is specified by the amplitudes A_{40} and A_{320} of the two signal components. These are updated every 25 ms. A virtual tactile surface is specified in terms of an amplitude map for each of the two frequency components that make up the stimulus.

The spatial resolution available from pacinian receptors is expected to be worse than that available from non-pacinian receptors, i.e., spatial discrimination for 320 Hz stimuli is expected to be worse than spatial discrimination for 40 Hz stimuli. In fact, results from psychophysics experiments on this type of array [SCS*01, SC02] suggest the converse: spatial discrimination is better for perception of stimuli at 320 Hz than at 40 Hz. Thus, although it seems likely that different receptor mechanisms are targeted by the different stimulation frequencies, there is some doubt about which receptor populations are involved.

4.4 Tactile rendering

As outlined above, during exploration of a virtual tactile environment a drive waveform is specified for each contactor of the stimulator array(s). The intention is to produce time-varying excitation patterns in the various populations of mechanoreceptors in the skin, so as to reproduce the touch sensations which are experienced during "real" tactile exploration.

A significant problem is the current lack of knowledge on the origin and nature of excitation patterns in real situations of tactile exploration of an object. The mechanical stimulation of a given receptor has a complicated relation to the mechanical properties and topology of the object's surface, to the mechanical properties of the skin and its local topology (especially skin ridges, i.e., fingerprints), and to the precise nature of the exploratory movement (speed, contact pressure and direction). Although it may be possible to produce an accurate software model of an object's surface, it is not at present possible to augment this with an accurate model of the skin/surface interaction. This situation may change in the near future: research is currently underway to develop an "artificial finger" with embedded transducers to mimic mechanoreceptors; improved finite-element models may also provide useful data.

For the particular case of the manipulation of textiles, the situation is more promising: Information on the nature of the mechanical input to the skin's mechanoreceptors is available from the Kawabata system for evaluation of textiles [Kaw80]. This provides a range of data on the textile sample under test, including surface roughness and surface friction profiles which are direct measures of the mechanical excitations produced when a probe is moved over the textile surface. The probe and associated instrumentation are designed so that the measured quantities correlate well with subjective assessment of the textile surface. Hence the Kawabata surface measurements provide an approximation to the "perceived surface", i.e., the surface after it has been "filtered" through the surface/skin interface. They thus provide a good basis for specifying drive signals for a stimulator array, in order to provide the tactile component for a virtual textile. Kawabata measurements have been used in this way by Govindaraj *et al.* [GGR*03]; they have also been used to provide source data for the tactile rendering developed within the HAPTEX project.

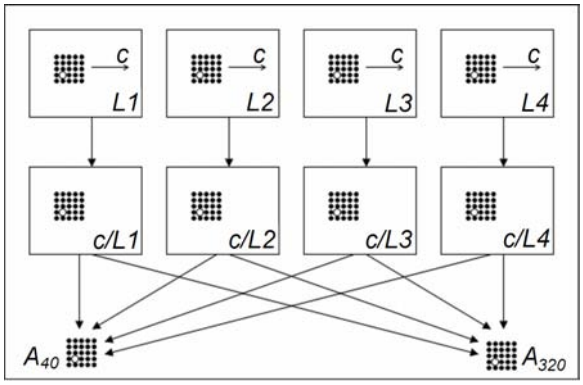

Figure 19: *A simple scheme for tactile rendering.*

Figure 19 outlines a simple scheme for tactile rendering, by which the drive signal to each point in the stimulator array is specified in terms of amplitude A_{40} at 40 Hz and an amplitude A_{320} at 320 Hz, and these amplitudes are in turn specified by the interaction between the virtual object and the exploratory movements of the user. The rendering is based on a pseudo-topology (i.e., an estimate of the surface after it has been filtered through the surface/skin interface), described in terms of amplitude distributions at length

scales *L1*, *L2*, etc.. These may be considered as amplitude distributions in frequency ranges *c/L1*, *c/L2*, etc., where *c* is the speed of exploration. [For a stimulator array with 2 mm spacing, the amplitude distributions might be specified at a resolution ("pixel size") of 1 mm, with effective feature widths of ≥ 2 mm.] For each point in the array, e.g., the point indicated by a white dot in Figure 19, the amplitudes in the different frequency ranges are combined by appropriate filter functions to produce the drive amplitudes A_{40} and A_{320}.

A similar rendering scheme developed within the HAPTEX project is summarised in Figure 20. For each digit, the tactile renderer generates 24 drive signals for the 24 contactors of the stimulator array. Input and output data specified in 25 ms timesteps. The input data are:

- a small-scale description of the object surface, represented as 2D *k*-space, derived from a pseudo-topology at 0.1 mm resolution over an area of a few mm^2;
- a large-scale description of the object surface: a representation of the non-uniformity of the surface, specified as pseudo-amplitudes at 1 mm resolution over an area of several tens of cm^2;
- position and orientation of the finger pad on the virtual surface;
- speed and direction of the movement of the finger pad over the virtual surface.

The operation of the renderer is as follows:

Taking account of the direction of movement, a spatial-frequency spectrum is calculated from the 2D *k*-space of the small-scale description of the virtual surface. Information about the speed of movement of the finger pad is used to convert spatial-frequency components into temporal-frequency components. The resulting temporal-frequency spectrum is reduced to only two amplitudes, A_{40} and A_{320}, by application of appropriate bandpass filter functions, corresponding to the 40-Hz and 320-Hz channels. (It should be noted that the signal-processing operations to this point may be performed only once per 25-ms timestep, i.e., they may be common to all 24 output channels.) Amplitudes for the 40-Hz component in the drive signals for each of the 24 channels are obtained from A_{40} by weighting according to data from the large-scale description of the virtual surface, for the 24 locations on the finger at which the contactors of the tactile stimulator are positioned. Similarly, amplitudes for the 320-Hz component in the drive signals for each of the 24 channels are obtained from A_{320} by weighting according to data from the large-scale description of the virtual surface. (Note that, in principle, different large-scale descriptions of the virtual surface may be used in the 40-Hz and 320-Hz channels, to allow for the observed difference in spatial resolution on the fingertip at the two frequencies.)

4.5 Discussion

When using stimulator arrays and rendering schemes as described above, the intention is to present time-varying spatial patterns of tactile stimuli which have two perceptual dimensions: one relating to intensity and one relating to spectral distribution. In order to establish the potential for such a system, it is necessary to determine whether a two-dimensional perceptual space can indeed be created in this way – it is very likely that the intensity dimension is available to the user, but less obvious that the spectral dimension is available. (A spectral dimension is available in the case of passive perception via a single contactor [She85, BED89], but this observation is not necessarily transferable to the case of active perception via an array of contactors.) However, recent results from Kyung *et al.* [KK07] demonstrate that test subjects can detect changes of frequency when stimuli are presented via a stimulator array in an active task, so it seems that spectral information is indeed available in such a scenario.

Initial evaluations of the HAPTEX system (Figure 20) also suggest that a 2D perceptual space can be achieved. For uniform stimuli (i.e., stimuli with no spatial variation over the skin), the spectral dimension appears relatively weak – changes in spectral balance at constant subjective intensity tend to be less noticeable than changes in subjective intensity at constant spectral balance. (There are perhaps 4 to 5 discriminable steps of spectral balance along an equal-intensity contour.)

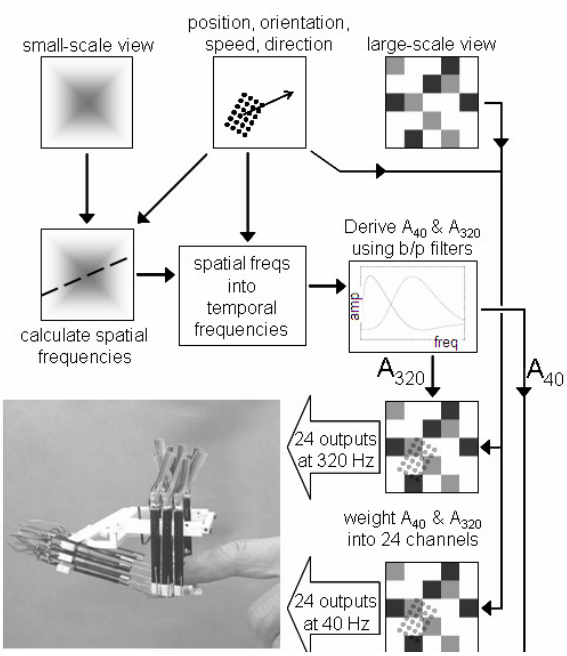

Figure 20: *The tactile renderer. Input and output data are specified in 25 ms timesteps.*

Perhaps the most interesting observation when using the HAPTEX system is a strong interaction between the perceived spatial aspects of the texture and the stimulation frequency. If the stimulation frequency is changed from 40 Hz to 320 Hz, the perceived sensation during active exploration changes much more if the texture is spatially non-uniform than if it is spatially uniform. It is clear that the spectral dimension provides a significant enhancement to the available range of tactile sensations.

Using data from the Kawabata system for a selection of real fabrics, the HAPTEX system has been used to simulate the tactile aspects of those fabrics. Given the apparent mismatch between the real situation (fingertip touching a textile) and the virtual situation (fingertip touching the metallic contactors of a stimulator array), results are surprisingly good – in some cases test subjects are able to match real and virtual textiles in terms of their tactile qualities. Prospects appear encouraging for the development of virtual textiles with acceptable tactile properties and it

seems likely that similar techniques can be successfully applied to other types of virtual object.

5. Force Feedback Technologies for the Rendering of the Direct Interaction with Deformable Objects

When addressing the problem of developing suitable force feedback technologies for the realistic haptic rendering of the physical interaction with deformable objects, a major distinction has to be recognized among the cases of "indirect interactions", i.e. interactions mediated by tools held by the user (for example in the case of the simulation of surgical operations) and the cases of "direct interactions", in which the limbs and the skin of the user come directly in contact with the surface of the deformable object, for example in the case of rubbing a textile. The latter case poses technical challenges that are dramatically more demanding than the former from both the qualitative and quantitative points of view. In this section we illustrate three examples of research works that aim at the improvement of the quality of direct contact simulation. These themes deal with the three important aspects of design of novel force feedback systems, innovative concepts for curvature simulation and control algorithms for accuracy improvement.

5.1 Introduction

While the simulation of the indirect interaction can satisfactory be addressed using an accurately force controlled robotic manipulator, having an end-effector shaped like the tool used in the simulation (for example a cutter, see Figure 21), the realistic simulation of the direct interaction implies the development of suitable technologies, able to comply with the extremely sensitive and sophisticated human haptic sensorial system that can perceive a large number of features characterizing the local contact with the object, like for example the global location/orientation with respect to the skin of the contact area(s) and its (their) extension, the local mechanical impedance(s) of the object (i.e. the relationship between the local displacement, speed, acceleration and the corresponding reaction force), the local large scale (e.g. the curvature), medium scale (e.g. bumps and edge) and small scale (e.g. the roughness) geometry, the local temperature, etc. (see Figure 22).

Figure 21: *Picture of a force feedback device for the simulation of indirect interactions.*

The mechanisms underling the perception of these features are currently not well understood and large research efforts are still required for identifying the stimuli that have to be generated in order to elicit the perception of a specific contact feature. The exploitation of haptic illusions seems a promising approach for the simplification of the stimuli to be generated, but also in this case in depth researches are needed for clarifying the quantitative dependencies of the equivalent stimuli with the intended perception to be elicited.

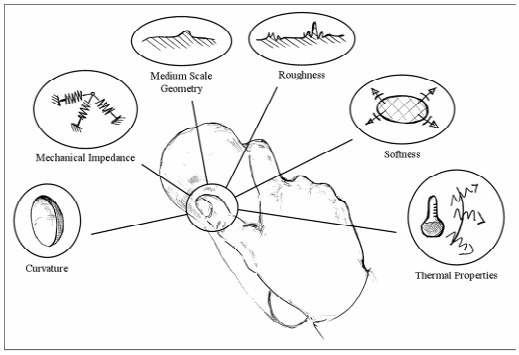

Figure 22: *Elements characterizing the local direct contact with a deformable object.*

As a broad result of the psychophysics researches carried on up today on the human haptic sensorial system, it can be said that there is a clear evidence of the major role of the mechanoreceptors located in the skin in the perception of the contact features, even if the proprioceptive sensors located in the physiological joints and in the tendons are used by the brain for the reconstruction of the global geometry and characteristics of the object, by space integration of the local perceptions.

From the technical point of view, the most accepted conceptual scheme for an haptic interface, able to render the direct interaction with virtual deformable objects, envisages the integration of a number of tactile arrays, i.e. a relatively high spatial resolution array of pins movable normally to a specified fixed surface in a relatively small range of motion, mounted on the end effectors of a force feedback device, i.e. an actuated and sensed mechanism able to move its end-effector(s) in a relatively large workspace and to generate controlled forces on it (them).

The first step in the definition of the requirements of the two different devices is the attribution of their roles in the generation of the required stimuli.

The most straightforward approach is to ascribe to the force feedback device the role of providing the means for the perception of the global characteristics of the local contacts, such as the locations/orientations of the contact areas with respect to the skin and their mechanical impedances, while the tactile actuator should be in charge of generating the stimuli that can change inside the contact area, like for example the small and medium scale geometry and the temperature. This approach live undefined the attribution of the generation of some border features like for example the global curvature and the extension of the contact area (that in fact in some way are each other dependent). In principle the global curvature of the local contact could be reproduced by the tactile array, but due to possible limitations to the maximum available displacement of the pins the alternative solution envisaging a global deformation of the surface where the pins are located should be also considered (see Figure 23).

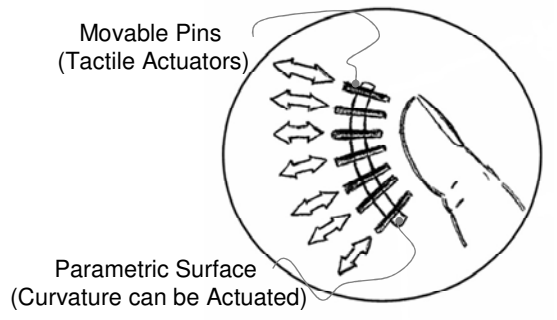

Figure 23: *Scheme of a the tactile array with deformable backing surface for the simulation of different local curvature*

Focusing on the basic functional requirements of the force feedback device, on the basis of what discussed above they can defined as the followings:

1. allow the modification of both the global location and the orientation of the contact areas (and therefore of the tactile arrays) with respect to the user's skin;

2. allow the modification of the global mechanical impedances of the contact areas. This implies the generation of global reaction forces in function of the global displacement of the contact area

It is worth to add some additional considerations and requirements in order to better understand the terms of the challenge and identify the major technological components that have to be developed.

The first point is to define how many independent contact areas should be managed at the same time by the device. In the general case, during an interaction with a deformable object a virtually infinite number of independent contact areas can be simultaneously generated (let's think for example to the case of the manipulation of a textile with the whole hand). This is clearly very far from being concretely achievable with the present technology and a reasonable simplification is required. Considering that the hand is the most important organ of human haptic exploration of the external word and that the fingertips are the most sensitive portions of the hand's skin, a reasonable simplification is to require that the device could manage simultaneously at least five independent contact areas, one for each fingertip. Furthermore, in order to exploit at best the sensitivity of the mechanoreceptors, the device should be able of reproducing the transition from the non-contact to the contact phases, i.e. the stimuli have to be generated only when a contact with the virtual object is detected.

The second point is to define the level of accuracy required for the generation of the controlled forces. Considering the high sensitivity and resolution capability of the mechanoreceptors in the skin and that many of the potential applications of the envisaged visual-haptic VR system, like for example the on line marketing of newly produced textiles/garments, would require the possibility of discerning very fine differences of the rendered features, the device should be able to accurately control global interaction forces that can be of the order of few centi-newtons (1 gf).

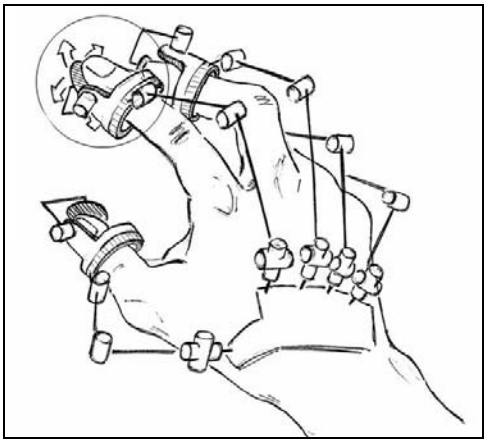

Figure 24: *Conceptual scheme of a force feedback device intended for the simulation of the direct interaction with the 5 fingertips of the hand.*

Finally, the device should allow as much as possible a natural interaction with the virtual object, posing minor limitations and constraints to the dexterity of the human hand and arm movements. This strongly suggests the adoption of an anthropomorphic configuration for the device structure that could be worn on the user's hand. All these requirements could be attained by the device whose conceptual scheme is sketched in Figure 24.

The device would be composed by 5 independent exoskeletons, each having 5 Degree of Freedoms (DoFs), 3 DoFs for positioning and 2 DoFs for orientating the end plate supporting the tactile actuator. Furthermore each exoskeleton would be equipped with a contactless position sensor for the tracking of the fingertip during the non contact phase and by a an accurate explicit force control that makes use of a 3 component force sensor providing the exact measure of the global resultant force delivered to the fingertips through the contact area.

In short the envisaged device would have a total of 25 actuated a position sensorised degrees of freedom, 5 force sensors each having at least 3 component measure capability and 5 contactless position sensors with at least 3 component measure capability. This huge number of components should be integrated in a compact device that can be easily worn by the user, without limiting the natural motion capability of the hand. This sets clearly the terms of the technological challenge.

With respect to the state of art, in order to attain the envisaged device three main technological areas have to be investigated:

1. The development of a compact anthropomorphic hand exoskeleton able to track the fingertip movements;

2. The development of an encountered haptic interface for the fingertip able of changing the position and orientation of a plate end effector with respect to the fingertip skin according to the local geometry of the virtual object and able to render the transition from the non-contact to contact phases;

3. The development of an accurate explicit force control and related force sensor.

All these major technological areas are under investigation at PERCRO. The attained results are described in the following paragraphs.

5.2 Development of the hand exoskeleton

A Hand Exoskeleton (HE) is a device able to exert forces on the phalanxes of the fingers. Several works (for example [VT99] and [BPBB02]) have addressed the development of different kinds of HEs.

Basically two types of HE can be identified in literature:

- *Multi-phalanx:* are multipoint devices where the force are exerted on each phalanx of the finger; each exerted force is directed along a fixed direction (normal to the phalanx)

- *Single Phalanx:* the device exchange forces only on the distal phalanx (the fingertip) of the finger; in this case the force has 3DoF and can be exerted in any wanted direction.

In our application, since the attention is focused on the fingertip area, a Single Phalanx 3DoF device has been realized.

The device uses quasi-anthropomorphic kinematics. This solution allows exploiting the benefits of anthropomorphic kinematics like maximum ratio of the available over the needed workspace and minimum encumbrance of the linkages. At the same time it is not perfectly anthropomorphic in order to avoid the singularity that would occurs when the finger is all extended. In Figure 25 a CAD model of the HE is shown. It can be noticed that the encumbrance of the device has been located in the dorsal side of the hand (except for the fingertip indeed) with the aim of allowing the complete closing of the hand. This has been achieved through the use of Remote Centre of Rotation mechanisms. These mechanisms are able to implement a rotational joint having an axis located outside the linkages.

The whole mechanism has 4DoF but it is actuated with only three motors thanks to the coupling of the last DoF (end-effector Joint) with the previous one. The coupling is acceptable because also in the human hand the last phalanx can be rarely moved independently from the middle phalanx during natural movements.

The HE is equipped with three electrical motors with low speed reduction ratios (1:14). The actuators are placed at the base of the mechanism in proximity of the dorsal side of the palm. The joints are actuated through in tension steel cable transmissions.

The position sensing is achieved with common encoders located on the axis of the motors and the force sensing is achieved with a purposely developed 3DoF force sensor placed at the end effector.

A purposely developed electronics for the sensor acquisition and the driving of the motors has been located inside the motor box at the base of the mechanism.

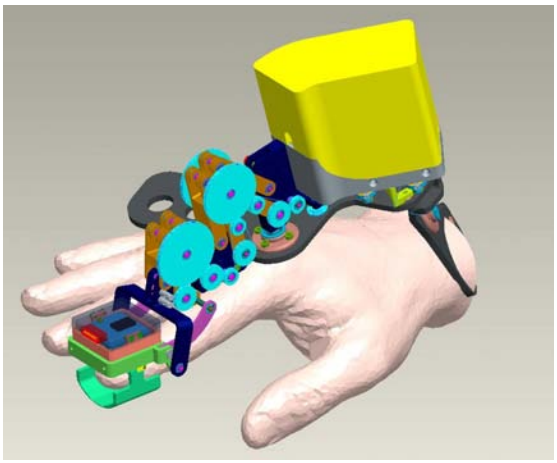

Figure 25: *CAD model of the Hand Exoskeleton*

This activity has been performed in the framework of the EU funded RTD Project HAPTEX (HAPtic rendering of virtual TEXtiles)

5.3 Development of an encountered haptic interface

Haptic interaction allows to naturally perform both haptic exploration of shapes/surfaces and active manipulation of objects. Nevertheless shape recognition isn't efficient if only kinaesthetic cues are provided. The restriction imposed on the fingertip contact region can blunt the haptic perception of shape and so local haptic cues play an important role in haptic perception of shape [JM06].

In [DH05] it is demonstrated how curvature discrimination can be carried out through a device providing only directional cues at the level of the fingertip, without any kinaesthetic information and moreover with a planar motion of the finger. This concept is also exploited to build robotic systems that can orient mobile surfaces on the tangent planes to the virtual object that is simulated, only at the contact points with the finger [DH05].

The system developed at PERCRO is composed of an encountered haptic interface. The basic concept for this type of devices was introduced in [SYYM04]. Our device is mounted on a kinaesthetic haptic interface, according to the overall configuration shown in Figure 26.

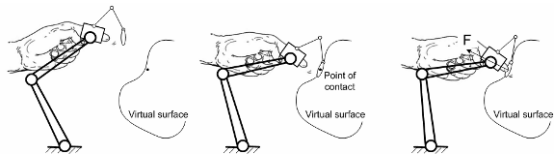

Figure 26: *Conceptual scheme of the developed encountered haptic interface*

In order to describe the working principle of the device, let's consider the case in witch the user is interacting with the virtual object: when the finger is far from the surface of the object, the plate of the fingertip haptic interface is kept far apart from the fingertip. When the finger touches the virtual surface, the plate comes into contact with the fingertip with an orientation determined by the geometric

normal of the explored surface. Simultaneously a reaction force, proportional to the penetration, is exerted by the supporting kinaesthetic haptic interface.

The supporting haptic interface is a pure translational parallel manipulator with three degrees of freedom (DoF).

The end-effector is connected to the fixed base via three serial kinematics chains (legs), consisting of two links connected by an actuated revolute joint and two universal joints at the leg end. The design of the device was optimized in order to minimize the friction forces and the inertia of the moving parts, obtaining the required transparency of the mechanism during the haptic exploration.

The actuation is realized by three brushed DC motor through a in tension steel cable transmission, characterized by low friction and zero backlash.

The encountered haptic interface was devised to bring the final plate into contact with the fingertip with different orientations and positioning with respect to the fingertip skin, according to the local geometry of the surface of the virtual object in correspondence of the contact point. These requirements have been met using a 5 DoFs kinematics, three of them (translational) devoted to the positioning in space of the end plate and the two others (rotational) for its orientation. A hybrid kinematics, consisting of a first parallel translational stage and a second parallel rotational stage, resulted the most suitable solution (Figure 27).

The translational stage has the same kinematics of the supporting haptic interface, with 3-UPU legs. In each leg the cable connected to the motor and a compression spring are mounted aligned to the centres of the universal joints. The spring works in opposition with the motor, in order to generate the required actuation force and to guarantee a pre-load on the cable.

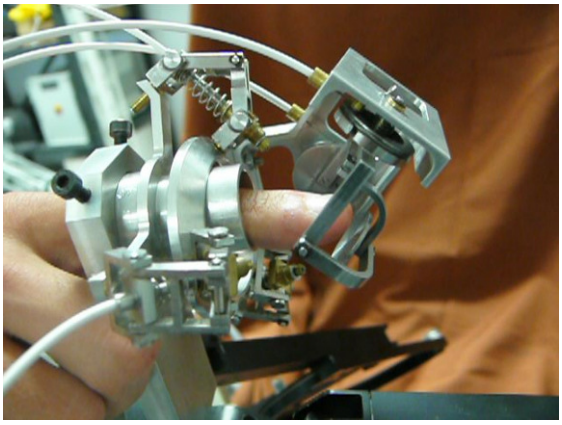

Figure 27: *Detail of the fingertip haptic interface*

The kinematics of the rotational stage allows the platform to rotate about two axis fixed to the translational stage.

Preliminary psychophysical tests have been carried on using the described system.

The method of constant stimuli for absolute threshold was employed for the discrimination of curvature by means of haptic cues. Four participants were recruited for this experiment. Each participant was informed about the procedure and did not present any dysfunction of the finger. They were experts on haptic interfaces but novices on this device. The test consisted in exploring a virtual surface with curvature varying from 0 m−1 (plane surface) to 6.67 m−1 (a sphere of radius equal to 150 mm). The observers were asked to answer to the question “is it a curved or a plane surface?”. The curvature values were 0, 1.82, 2.22, 2.86, 3.33, 4, 5, 6.67 m−1, and 100 stimuli were presented to each participant. The stimulus with a percentage of 50% of affirmative responses was considered as the threshold for detection of curvature. In Figure 28 is shown the device and a planar scheme of the haptic cues displayed to the users.

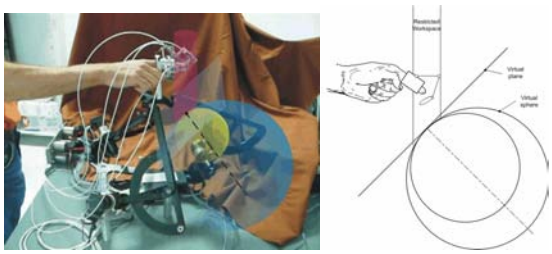

Figure 28: *Experimental set-up*

The test was carried out in two different modalities, A and B. In condition A both the kinaesthetic and the local geometry haptic cues were provided to the observers: the mobile platform of the fingertip device was kept in contact with the fingertip when the user was in contact with the surface, with an orientation tangent to the displayed virtual surface. In condition B only the kinaesthetic feedback was provided by the supporting haptic interface. In both modalities the haptic exploration was carried out in a restricted workspace, limited by a vertical cylinder with diameter of 25 mm.

The sigmoid curves for the two modalities are represented in Figure 29 for all the subjects, where the thresholds are pointed out, resulted using the fingertip haptic device (red line) and with the only kinaesthetic cues (blue line).

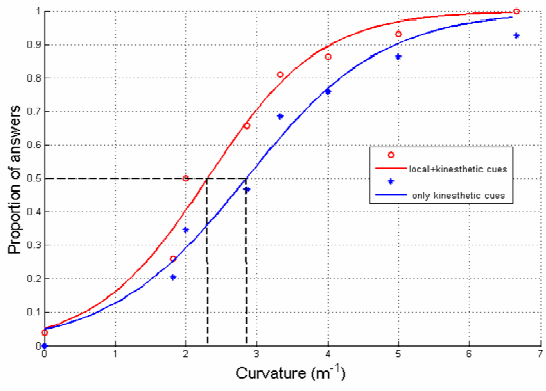

Figure 29: *Sigmoid curves for curvature threshold*

The average values of curvature threshold for the two conditions resulted respectively in 2.35±0.35 and 3.02±0.58 m−1, with an improvement of 22.2% in the performance for modality A.

Although the ANOVA between the two conditions do not reach a significant level (p=0.069), we can however presume that further investigations employing more accurate schemes and conditions, e.g. method of limits and

TSD, and carried out on a larger sample of subjects/points, may statistically point out this difference. The data are consistent with what has been already found in literature for discrimination of curvature, either using haptic interfaces or real objects.

This activity has been performed in the framework of the EU funded RTD Network of Excellence ENACTIVE.

5.4 Development of accurate explicit force control

The simulation of fine interaction, in which the exchanged forces are of the order of few grams, requires the implementation of highly accurate force feedback devices.

This could be achieved through a careful design of the mechanical component of the device. However, when the required workspace is large and the performances are demanding, it is necessary to introduce advanced control technique in order to compensate the unwanted resistant forces.

In this work we implemented a motion-based explicit force control algorithm using a force sensor located at the end-effector of a haptic device. The general architecture of this algorithm was introduced in [VK93]. The control is implemented on a device that was originally designed for open loop control, i.e. without force sensing.

The haptic device taken as reference for this work is the GRAB system (described in [AMA*03]) developed by PERCRO Laboratory in the framework of the homonymous European RTD Project. GRAB is a 6 DoFs desktop force-feedback device with a serial kinematics. The first 3 DoFs (RRP) are required to track the position of the fingertip in 3D space and the remaining 3 (RRR) are required to track its orientation. The first 3 DoFs are actuated in order to exert forces of arbitrary orientation at the fingertip, whereas the last 3 DoFs are passive and are realized by a gimbal. On the last DoF of the gimbal a thimble is mounted for the connection to the user's fingertip. The 3 motors are remotely located: the first 2 actuators are mounted on the fixed link (base), while the third actuator is mounted on the second moving link. Forces are transmitted from the actuators to the joints by in tension metallic tendons routed on idle pulleys. There are no geared reducers and the motors are sensorised by optical encoders. For implementing explicit force-feedback control, a commercial 6-components force sensor from ATI (NANO17) has been placed at the base of the gimbal.

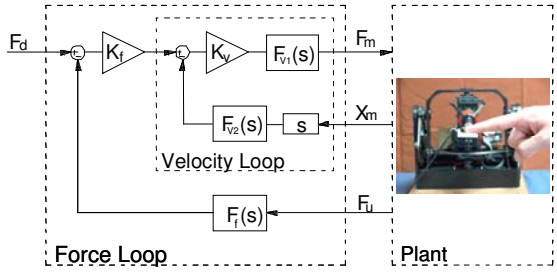

Figure 30: *Scheme of the force control*

The 1 DoF scheme of the controller is represented in Figure 30: it consists of an inner velocity loop-outer force loop scheme. This one-dimensional scheme can be simply generalized for implementing a three dimensional force control: it's sufficient to transform the velocity reference, obtained as output of gain K_v, in a joint speed reference by simply multiplying it for the inverse of Jacobian matrix, which describe the inverse differential kinematics of device. This solution allows general control architecture to be safe and simplify the interface procedure with user.

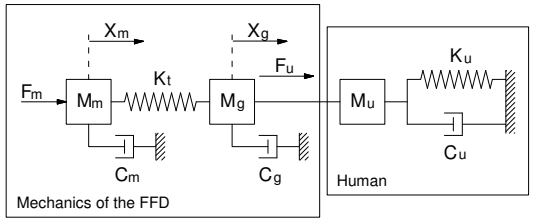

Figure 31: *Mechanical model*

The proper dimensioning of such controller required the following step:

- Building of a dynamic model of the mechanical system: the 1 DoF model (Figure 31) has been taken as reference; this model was experimentally validated.

- Estimation of the user impedance. The impedance of the finger in a thimble has been experimentally measured since it has a strong influence on the stability of the loop.

The design of the controller was carried on focusing on the inner velocity loop first. Two filters were introduced for the velocity loop:

1) a third order Chebyshev Type I for guaranteeing the stability of the velocity loop

2) a filter for velocity signal (velocity signal generated by digital encoders)

The outer force loop was then designed.

A Butterworth filter was introduced to guarantee the stability.

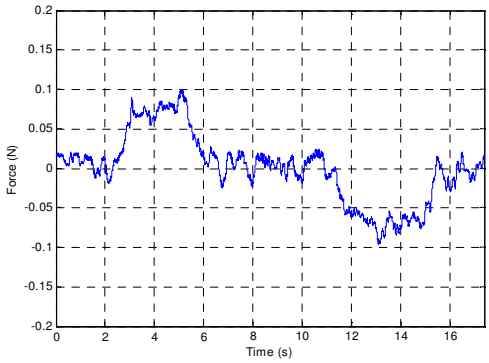

Figure 32: *Plot of the resistant force versus time during finger tracking at constant velocity*

A field test investigating the system capability to track the finger motion has been carried on. The subjects were asked to move their fingers at constant velocity and the system was set to display no forces. The maximum module of the acquired resistant force was about one tenth of Newton (10 grams force), as it can be observed in Figure 32.

This activity has been carried on in the framework of the EU funded RTD Project HAPTEX (HAPtic rendering of virtual TEXtiles)

5.5 Conclusion and future works

The development of force feedback technologies suitable for the rendering of the direct interaction with deformable objects is a tremendously challenging activity due to the very sophisticated capability of the human haptic sensorial system.

A reference configuration for the device addressing the case of direct interaction with the five fingertips of the hand has been identified. The three main technological areas required for attaining the envisaged device, namely the development of a compact anthropomorphic hand exoskeleton, the encountered haptic interface techniques, the accurate explicit force control and the compact 3 component force sensor, are now under investigation at PERCRO and the preliminary results are encouraging. The next research goal will be the integration of all the developed technologies in a single compact device.

6. Acknowledgments

The project "HAPTEX - HAPtic sensing of virtual TEXtiles" (Contract Nr.: IST-6549) is funded by the Sixth Framework Programme (FP6) of the European Union.

References

[AMA*03] AVIZZANO C. A., MARCHESCHI S., ANGERILLI M., FONTANA M., BERGAMASCO M.: A Multi-Finger Haptic Interface for Visually Impaired People. In *Proceedings of the 2003 IEEE International Workshop on Robot and Human Interactive Communication,* Vol. 31, (2003), 165- 170.

[AH98] ASTLEY, O. R., HAYWARD, V., "Multirate haptic simulation achieved by coupling finite element meshes through Norton equivalents", *Robotics and Automation, 1998. Proceedings.* IEEE, vol. 2, 16-20 May 1998 989 – 994, 1998.

[BED89] BERNSTEIN L. E., EBERHARDT S. P., DEMOREST M. E.: Single-channel vibrotactile supple-ments to visual perception of intonation and stress. *J. Acoust. Soc. Am. 85*, (1989), 397–405.

[BHA*03] BENALI-KHOUDJA M., HAFEZ M., ALEXANDRE J. M., KHEDDAR A.: Electromagnetically Driven High-Density Tactile Interface Based on a Multi-Layer Approach. *International Symposium on Micro-mechatronics and Human Science (MHS 2003)*, 147–152, 2003-

[BHW94] BREEN D.E., HOUSE D.H., WOZNY M.J.: Predicting the Drape of Woven Cloth Using Interacting Particles, Computer Graphics (ACM SIGGRAPH 94 proc.), Addison-Wesley, pp 365-372, 1994.

[BMF03] BRIDSON R., MARINO S., FEDKIW R., 2003, Simulation of Clothing with Folds and Wrinkles, Eurographics-SIGGRAPH Symposium on Computer Animation, pp 28-36.

[BPBB02] BOUZIT M., POPESCYU G., BURDEA G., BIOAN R.: The Rutger Master II-nd Force Feedback Glove, In *Proc. IEEE Vr. Haptic Sysmposium*, Vol.7 (March 2002) 256-263.

[BW98] BARAFF D., WITKIN A.: Large Steps in Cloth Simulation, Computer Graphics (SIGGRAPH'98 proceedings), Addison-Wesley, 32, pp 106-117, 1998.

[BWH*06] BERGOU M., WARDETZKY M., HARMON D., ZORIN D., GRINSPUN E.: A Quadratic Bending Model for Inextensible Surfaces, Proc. of Eurographics Symposium on Geometry Processing, pp 227-230, 2006.

[CK02] CHOI K.J., KO H.S.: Stable but Responsive Cloth, Computer Graphics (SIGGRAPH'02 proceedings), Addison Wesley, 2002.

[CSB*06] CORNES N. L., SULLEY R., BRADY A. C., SUMMERS I. R.: Measurements on pacinian corpuscles in the fingertip. *Proc. Enactive'06*, Montpelier, (2006), 117–118.

[DH05] DOSTMOHAMED H., HAYWARD V.: Trajectory of contact region on the fingerpad gives the illusion of haptic shape. *Experimental Brain Research 164*, Vol.3 (2005), 387–394.

[DSB99] DESBRUN M.,.SCHRÖDER P, BARR A.: Interactive Animation of Structured Deformable Objects, Proceedings of Graphics Interface, A K Peters, 1999.

[EDC96] EISCHEN J.W., DENG S., CLAPP T.G.: Finite-Element Modelling and Control of Flexible Fabric Parts, Computer Graphics in Textiles and Apparel (IEEE Computer Graphics and Applications), IEEE Press, pp 71-80, Sept. 1996.

[EEH00] EBERHARDT B., ETZMUSS O., HAUTH M.: Implicit-Explicit Schemes for Fast Animation with Particles Systems, Proceedings of the Eurographics workshop on Computer Animation and Simulation, Springer-Verlag, pp 137-151, 2000.

[EGS03] ETZMUSS O., GROSS J., STRASSER W.: Deriving a Particle System from Continuum Mechanics for the Animation of Deformable Objects, IEEE Transactions on Visualization and Computer Graphics, IEEE Press, pp 538-550, 2003.

[ES87] EPPINGER S., SEERING, W.: Understanding bandwidth limitations in robot force control. In *Proc.Robotics and Automation.Conference*, *1987 IEEE International Conference on* , Vol.4 (1987), 904- 909.

[EWS96] EBERHARDT B., WEBER A., STRASSER W.: A Fast, Flexible, Particle-System Model for Cloth Draping, Computer Graphics in Textiles and Apparel (IEEE Computer Graphics and Applications), IEEE Press, pp 52-59, Sept. 1996.

[FMF*92] FORMBY, C., MORGAN, L. N., FORREST, T. G., RANEY, J. J.: The role of frequency selectivity in measures of auditory and vibrotactile temporal resolution. *J. Acoust. Soc. Am. 91,* (1992), 293–305.

[GBH01] GESCHEIDER G. A., BOLANOWSKI S. J., HARDICK K. R.: The frequency selectivity of information-processing channels in the tactile sensory system. *Somatosensory And Motor Research 18*, (2001) 191–

201.

[GGR*03] GOVINDARAJ M., GARG A., RAHEJA A., HUANG G., METAXAS D.: Haptic simulation of fabric hand. *Proc. Eurohaptics '03*, Dublin, (2003), 253–260.

[GHDS03] GRINSPUN E., HIRANI A., DESBRUN M., SCHRÖDER P., 2003, Discrete Shells, ACM Symposium on Computer Animation, ACM Press.

[GPU*03] GOVINDARAJ, M., PASTORE, C., UPADHYAY, A., METAXAS, D., HUANG, G., RAHEJA, A.: Haptic simulation of fabric hand. Technical report, *National Textile Research Annual Report*, 2003.

[Hap05a] HAPTEX CONSORTIUM, "System Requirements and Architectural Design", HAPTEX Deliverable D1.1, http://haptex.miralab.unige.ch/, 2005

[Hap05b] HAPTEX CONSORTIUM, "First set of measurements", HAPTEX Deliverable D3.1, http://haptex.miralab.unige.ch/, 2005

[Hap06a] HAPTEX CONSORTIUM, "Specification of the Whole Haptic Interface", HAPTEX Deliverable D4.1, http://haptex.miralab.unige.ch/, 2005

[Hap06b] HAPTEX CONSORTIUM, "Separate Haptic and Tactile Interface", HAPTEX Deliverable D4.2, http://haptex.miralab.unige.ch/, 2005

[HB04] HAFEZ M., BENALI-KHOUDJA M.: 3D Tactile Rendering Based on Bi (Multi) stable SMA Monolithic Systems. *International Symposium on Micro-mechatronics and Human Science (MHS 2004)*, (2004), 93–98.

[HE01] HAUTH M., ETZMUSS O.: A High Performance Solver for the Animation of Deformable Objects using Advanced Numerical Methods, Eurographics 2001 proceedings, Blackwell, 2001.

[Hua02] HUANG, G.: Feel the fabric via the phantom. *PhD thesis*, University of Pennsylvania, 2002.

[JYV00] JOHNSON K. O., YOSHIOKE T., VEGA-BERMUDEZ F.: Tactile functions of mechanoreceptive afferents innervating the hand. *J. Clin. Neurophysiol. 17*, (2000), 539–558.

[JM06] JANSSON G. , MONACI L.: Identification of real objects under conditions similar to those in haptic displays: providing spatially distributed information at the contact areas is more important than increasing the number of areas. *Virtual Reality 9*, Vol.4 (2006), 243–249.

[KAK*06] KYUNG K. U., AHN M., KWON D. S., SRINIVASAN M.A.: A compact planar distributed tactile display and effects of frequency on texture judgement. *Advanced Robotics 20*, (2006), 563–580.

[Kaw80] KAWABATA, S.: The standardization and analysis of hand evaluation, 2nd ed. The hand evaluation and standardization committee, *The Textile Machinery Society of Japan*, Osaka, 1980.

[KBD*07] KILLEBREW J. H., BENSMAIA S. J., DAMMANN J. F., DENCHEV P., HSIAO S. S., CRAIG J. C., JOHNSON K. O.: A dense array stimulator to generate arbitrary spatio-temporal tactile stimuli. *Journal Of Neuroscience Methods 161*, (Mar. 2007), 62–74.

[KC02] KANG Y.M., CHO H.G.: Bilayered Approximate Integration for Rapid and Plausible Animation of Virtual Cloth with Realistic Wrinkles, Computer Animation 2000 proceedings, IEEE Computer Society, pp 203-211, 2002.

[KK07] KYUNG K. U., KWON D. S.: Perceived roughness and correlation with frequency and amplitude of vibrotactile frequency. *Proc. Eurohaptics '06*, Paris (2006), 277–282.

[LPH07] LEVESQUE V., PASQUERO J., HAYWARD V.: Braille Display by Lateral Skin Deformation with the STReSS^2 Tactile Transducer. *Proc. World Haptics '07*, Tsukuba, (2007), 115–120.

[MDDB00] MEYER M., DEBUNNE G., DESBRUN M., BARR A. H., Interactive Animation of Cloth-like Objects in Virtual Reality, Journal of Visualization and Computer Animation, John Wiley & Sons, 2000.

[MKE03] METZGER J., KIMMERLE S., ETZMUSS O.: Hierarchical Techniques in Collision Detection for Cloth Animation, Journal of WSCG, 11 (2) pp 322-329, 2003.

[MMLMT05] MÄKINEN M., MEINANDER H., LUIBLE C., MAGNANAT-THALMANN N.: Influence of physical parameters on fabric hand. In *Proc. HAPTEX'05 Workshop on Haptic and Tactile Perception of Deformable Objects* (2005).

[MTB06] MAGNENAT-THALMANN N., BONANNI U.: Haptics in Virtual Reality and Multimedia. *IEEE MultiMedia*, vol. 13, no. 3, pp. 6-11, Jul-Sept, 2006.

[PH03] PASQUERO J., HAYWARD V.: STReSS: A Practical Tactile Display System with One Millimeter Spatial Resolution and 700 Hz Refresh Rate. *Proc. Eurohaptics '03,* Dublin, (2003), 94–110.

[PVTF92] PRESS W.H., VETTERLING W.T., TEUKOLSKY S.A., FLANNERY B.P., Numerical Recipes in C, Second edition, Cambridge University Press, 1992.

[RHD*87] RABINOWITZ W. M., HOUTSMA, A. J. M., DURLACH, N. I., DELHORNE, L. A.: Multi-dimensional tactile displays: Identification of vibratory intensity, frequency and contactor area. *J. Acoust. Soc. Am 82*, (1987), 1243–1252.

[SBS*05] SUMMERS I. R., BRADY A. C., SYED M., CHANTER C. M.: Design of Array Stimulators for Synthetic Tactile Sensations. *Proc. World Haptics'05*, Pisa, (2005), 586–587.

[SC02] SUMMERS I.R., CHANTER C.M.: A broadband tactile array on the fingertip. *J. Acoust. Soc. Am. 112*, (2002), 2118–2126.

[SCS*01] SUMMERS I. R., CHANTER C. M., SOUTHALL A. L., BRADY A. C.: Results from a Tactile Array on the Fingertip. *Proc. Eurohaptics '01*, Birmingham, (2001) 26–28.

[She85] SHERRICK C. E.: A scale rate for tactual vibration. *J. Acoust. Soc. Am. 78,* (1985), 78–83.

[SFR*05] SALSEDO F., FONTANA M., RUFFALDI E., BERGAMASCO M., MAGNENAT-THALMANN N., VOLINO P., BONANNI U., BRADY A., SUMMERS I., QU J., ALLERKAMP D., BÖTTCHER G., WOLTER F.-E.,

MÄKINEN M., MEINANDER H.: Architectural design of the haptex system. In *Proc. HAPTEX'05 Workshop on Haptic and Tactile Perception of Deformable Objects* (2005).

[SWM*05] SUMMERS I. R., WHYBROW J. J., MILNES P., BROWN B. H., STEVENS J. C.: Tactile perception; comparison of two stimulation sites. *J. Acoust. Soc. Am. 118*, (2005), 2527–2534.

[SYYM04] SATO Y., YOSHIKAWA T., YOKOKOHJI Y., MURAMORI N.: Designing an encountered-type haptic display for multiple fingertip contacts based on the observation of human grasping behaviour. In *Proceedings of the Symposium on haptic interfaces for virtual environment and teleoperator systems*, (2004) 66-73.

[TW06] THOMASZEWSKI B., WACKER M.: Bending Models for Thin Flexible Objects, *WSCG Short Communication Proc.*, 9(1), 2006

[TWS06] THOMASZEWSKI B., WACKER M., STRASSER W., 2006, A Consistent Bending Model for Cloth Simulation with Corotational Subdivision Finite Elements, *Proc. of ACM-SIGGRAPH Symposium on Computer Animation 2006*, pp 107-116.

[Ver63] VERILLO R. T.: Effect of contactor area on the vibrotactile threshold. *J. Acoust. Soc. Am. 35*, (1963), 1962–1966.

[VDB*07] VOLINO P., DAVY P., BONANNI U., LUIBLE C., MAGNENAT-THALMANN N., MÄKINEN M., MEINANDER H.: From Measured Physical Parameters to the Haptic Feeling of Fabric. *The Visual Computer*, Springer Berlin/Heidelberg, vol. 23, no. 2, pp. 133–142. February 2007.

[VFS69] VERILLO R. T., FRAIOLI A. J., SMITH R. L.: Sensation magnitude of vibrotactile stimuli. *Perception & Psychophysics 6*, (1969), 366–372.

[VGV90] VAN DOREN C. L., GESCHEIDER G. A., VERRILLO R. T.: Vibrotactile temporal gap detection as a function of age. *J. Acoust. Soc. Am. 87*, (1990), 2201–2205.

[VK93] VOLPE R., KHOSLA P.: A theoretical and experimental investigation of explicit force control strategies for manipulators. In *IEEE Transactions on Automatic Control*, vol.38, 11 (1993), 1634-1650.

[VMT97] VOLINO P., MAGNENAT-THALMANN N.: Developing Simulation Techniques for an Interactive Clothing System, Virtual Systems and Multimedia (VSMM'97 proceedings), IEEE Press, Geneva, Switzerland, pp 109-118, 1997.

[VMT00] VOLINO P., MAGNENAT-THALMANN N.: Implementing fast Cloth Simulation with Collision Response, Computer Graphics International Proceedings, IEEE Computer Society, pp 257-266, 2000.

[VMT01] VOLINO P., MAGNENAT-THALMANN N.: Comparing Efficiency of Integration Methods for Cloth Simulation, Computer Graphics International Proceedings, IEEE Computer Society, 2001.

[VMT05] VOLINO P., MAGNENAT-THALMANN N.: Accurate Garment Prototyping and Simulation, *Computer-Aided Design & Applications*, 2(1-4), CAD Solutions, 2005.

[VMT06] VOLINO P., MAGNENAT-THALMANN N., 2006, Simple Linear Bending Stiffness in Particle Systems, Proc. of ACM-SIGGRAPH Symposium on Computer Animation 2006, pp 101-105.

[VT99] VIRTUAL TECHNOLOGIES INC.: *Cyber Grasp User Guide*, 1999.

[WLH02] WAGNER C. R., LEDERMAN S. L., HOWE, R. D.: A Tactile Shape Display Using RC Servomotors. *Proc. 10th Symposium on Haptic Interfaces for Virtual Environment and Teleoperator Systems*, Orlando, (2002), 354.

[WLH04] WAGNER C. R., LEDERMAN S. L., HOWE R. D.: Design and Performance of a Tactile Shape Display Using RC Servomotors. *Haptics-e: The Electronic Journal Of Haptics Research 3*, (2004).